

DOTTORATO DI RICERCA IN SCIENZE DELLA TERRA

Università degli Studi di Firenze



GIACOMO ULIVIERI

**“Dynamic model of the continuous degassing of the shallow
magmatic column at Stromboli volcano as inferred by
infrasonic data”**

settore scientifico disciplinare: GEO-10

Tutore: Prof. M. Ripepe

Coordinatore: Prof. F. Sani

XXI CICLO

Firenze, 31 Dicembre 2008

INDEX

1. Introduction	4
Persistent magma degassing	6
2. Methodology	10
Infrasound on volcanoes.....	10
Small aperture infrasonic array at Stromboli.....	15
<i>The Electret Condenser Infrasonic Sensors.....</i>	<i>17</i>
Analysis of infrasonic data by means of array	20
<i>Efficiency of the infrasonic array.....</i>	<i>23</i>
3. Infrasonic analysis of active degassing at Stromboli	26
Infrasonic explosions and puffing.....	26
Detection of intermittent infrasonic pulses	28
Parameters for active degassing derived from infrasonic data.....	33
<i>The active degassing regime</i>	<i>34</i>
<i>Insight on source and mass outflow</i>	<i>39</i>
<i>The behaviour of the source location</i>	<i>49</i>

4. The dynamic model of active degassing	53
Gas accumulation model	54
The proposed model for the shallow feeding dike at Stromboli	62
The transition from explosive to effusive in 2006-2007	64
<i>The propagation of a NE-SW dike and the drainage of magma from shallow conduits</i>	<i>68</i>
5. Conclusion	71
6. References.....	76

1. Introduction

Understanding the dynamics of active volcanoes has fundamental implications for modelling eruptive phenomena, and provides the basis for volcanic hazard assessment. Many different processes are observed on worldwide active volcanoes, such as the lava effusion, the pyroclastic flows, the wide spectrum of explosive activity ranging from mild strombolian to vulcanian and plinian explosive activity, and the continuous “quiescent” degassing. Besides the styles of activity are specific of a geodynamic context, the magma reology represents the main character influencing the activity style. In particular, when the magma approaches the shallow portion of the crust, the decrease of the confined pressure causes the mineral crystallization and the exsolution of endogenous gas, resulting in a multiphase (liquid+solid+gas phase) system. Volatiles in magma represent the engine of volcanic eruptions and play an important role in all the physical and chemical processes affecting the ascending magma from depth to the surface.

This work analyzes the dynamics of volcanic degassing with particular referring to persistent volcanism as observed on many active volcanoes worldwide. Persistent volcanism involves extensive thermal and volatile fluxes observed on different volcanoes at which degassing activity lasts from decades to centuries (e.g., Allard et al., 1994 and 1997). Lava lake and open vents degassing is observed at basaltic volcanoes (Francis et al., 1993; Allard et al., 1991) such as Erebus (Antarctica), Kilauea (Hawaii), Etna (Italy) and Stromboli (Italy). Long-lived, high-temperature fumarole fields are another expression of persistent degassing, as observed at quiescent volcanoes such as Momotombo and Masaya (Nicaragua, Menyailov et al., 1986; Stix, 2007) and active lava dome volcanoes such as Soufriere Hills, (Montserrat) and Mount S. Helens (Washington).

This thesis addresses the persistent Strombolian-type activity as observed at Stromboli volcano. This type of volcanic activity is observable on many open conduits, basaltic volcanoes worldwide (Etna, Italy; Erebus, Antartide; Shishaldin and Pavlov, Alaska; Villarica, Cile; Kilauea, Hawaii; Yasur, Vanuatu; Ekla, South Iceland; Karimsky, Kamtchatka Pensinsula) and represents one stage in the activity of basaltic volcanoes

through time (Druitt et al., 1989). This eruption style is characterized by periodic (minutes), mild gas-rich eruption of scoria and ash superimposed on a continuous degassing through open vents and/or fumarole fields. This volcanism, hence, reflects the dynamics of a continuous gas discharge of a shallow magma. At several volcanoes it occurs during the pre, post and sin eruptive phases and lasts from day to month, while at Stromboli represents the main style in the last ~1500-years (Rosi et al., 2000).

Persistent magma degassing

The process of magma degassing activity lasting for decades to centuries, requests an amount of melt depending on the concentration of volatiles. The volume of magma that fed the continuous degassing is generally calculated by dividing the released amount of magmatic gas by the gas content. Estimates of initial gas concentration in magmas are achieved from melt inclusions analysis in phenocrysts (Anderson 1974; Devine 1984). The results of such analysis give a lower limit for the content of volatile at the time of the melt inclusion. COSPEC (Correlation Spectrometer) is the most common tool for monitoring the degassing at volcanoes, and allows the quantitative measurement of SO₂ flux (Stoiber et al., 1983) in volcanic plume. SO₂ gas fluxes from lava lake and active strombolian vents during passive degassing activity, range from few kg/s (i.e., Stromboli, Erebus, Kilawea) up to tens of kg/s like at Etna (Table 1). Assuming 0.01-0.05 wt% sulphur content for basaltic to andesitic magmas (Gerlach and Graeber, 1985; Metrich et al., 2001), the volumes of magma supply to generate such fluxes, are in one year in the order 0.1-0.7 km³ for Stromboli, Kilawea and Erebus and up to 3-8 km³ for Mt. Etna.

Table 1. Some estimate of average SO₂ gas fluxes from persistent (years to decades), open vent volcanoes during passive degassing activity.

Volcano	SO ₂ flux (kg/s)	reference
Kilauea	2	<i>Gerlach et al., 1998</i>
Mt. Etna	50	<i>Bruno et al., 1999</i>
Stromboli	3	<i>Allard et al., 1994</i>
Erebus	5	<i>Zreda-Gostynska et al., 1993</i>

These volume estimates of the of degassed magma do not generally mach the magma being erupted in the same period (Andreas et al., 1991; Kazahaya et al., 1993; Francis et al., 1993), arising a fundamental volcanological problem of the excess of SO₂ degassing at persistent active volcanoes. The magmatic volatiles in excess moreover, are dominated by

water and sulphur, which are relatively soluble in silicate melts. A 0.4-4 MPa saturation pressure has been modelled for the most abundant SO₂ and H₂O gas species (Papale et al., 2005; Burton et al., 2007; Gerlach et al., 1986), corresponding to a lithostatic pressure less than 150 m, which indicates that these volatiles have evolved from shallow magma source. At such shallow depth geophysical analysis have never detected the presence of huge volumes of magma, which instead have been located at greater (> 5 km) depth, where most of volatiles are dissolved. The efficiency of magma degassing at persistent volcanoes, hence, cannot be explained in term of large shallow reservoirs.

A volcanic process that continuously supply gas-rich magma from depth but that not totally erupted has to invoke to model the sustained and long living gas discharge at volcanoes. This volcanological problem has been quantitatively solved with magma convection dynamics in volcanic conduits (Kazahaya et al., 1994; Stevenson and Blake, 1998), the schema of what is summarized in Figure 1. The difference in density between dense, shallow degassed and less dense, deep gas-rich magma, is the driving force for convective overturn. Laboratory experiment (Stevenson and Blake, 1998) indicates that, depending on magma viscosity ratio, convection can occurs by concentric flow of the magma along the conduit. The modelled gas flux is directly correlated with the viscosity ratio and is more likely possible for low-viscosity magmas. This model calculates the maximum H₂O and CO₂ fluxes that can be explained by the convection of gas-rich buoyant magma as a function of 1) magma composition (initial water content, crystal content and gas fraction), 2) temperature, 3) conduit radius, 4) magma chamber depth and 5) amount of degassed water. The model fits two end-member of degassing regimes: active dacitic magma degassing of dome system with a relatively gas-poor (CO₂) supply from a 7 km depth chamber (Mount St. Helens), and more efficient basaltic magma degassing with strombolian activity characterized by a gas-rich (1-4% volume of CO₂) magma supply from a 2 km depth chamber. In both cases, the sizes of shallow conduits requested for efficient convective circulation are relatively small (< 10 and 60 m, respectively) respect to the large dimensions of the shallow chamber requested if no convection occurs.

Degassing-induced convection provides, hence, an efficient mechanism for gas discharge of the shallow volcanic system at the expense of the volatile content of a deep magma chamber (Stevenson and Blake, 1998).

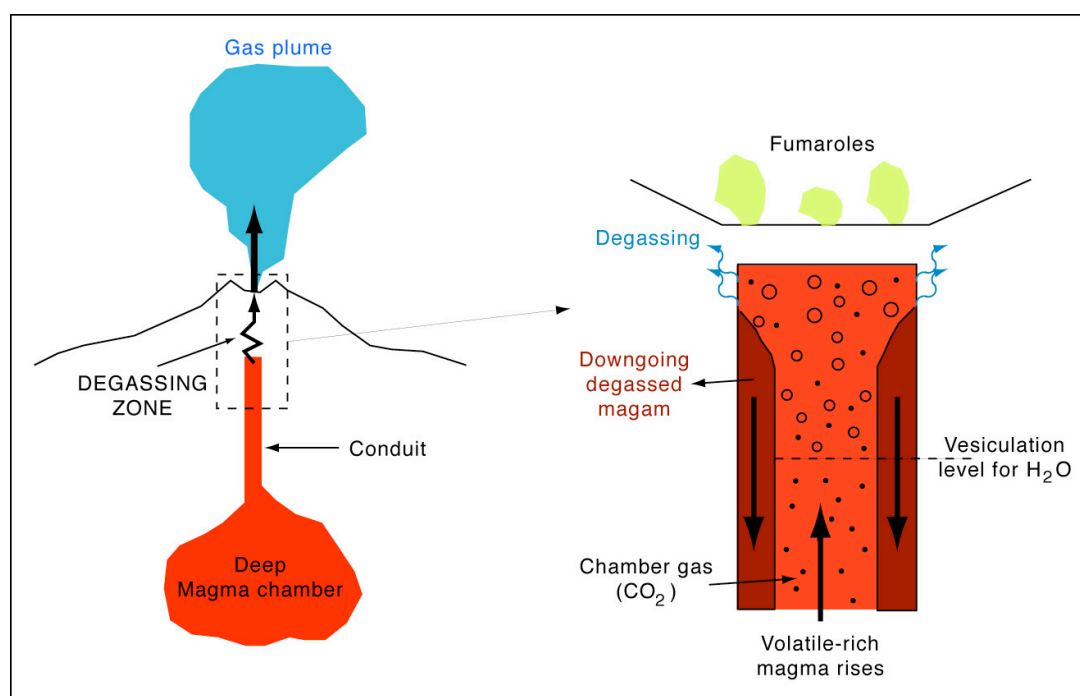


Figure 1. Convective degassing model from Stevenson and Blake (1988). A cylindrical conduit connects a deep magma chamber with relatively insoluble gases (CO_2) to shallow depths. At shallow level the more soluble gases (H_2O and SO_2) exsolve and together with less soluble CO_2 escape from the melt supplying a gas fluxes to the atmosphere. During ascent, the density difference between shallow degassed (high density) and deeper gas-rich (low density) magma drive a convective circulation system promoting efficient and long living magma degassing that explain the excessive gas fluxes on many persistent volcanoes worldwide.

In these calculations, gas emission rate is assumed to be equal to the gas supply rate in the shallow degassing zone (Figure 1). However, the way gas is lost is not taken into account and the magma convection is assumed to be the main rate-limiting process for gas discharge in the atmosphere. This assumption can be valid in the case of open vents basaltic volcanoes such as Stromboli, Masaya, Erebus and Izu-Oshima (Stevenson, 1992; Kazahaya et al., 1994). However, when the gas loss process segregates gas bubbles from melt the efficiency of gas discharge should increase, affecting significantly the convective degassing model. For this reason, the process of magma degassing has received a great attention in the scientific community, with several experimental and theoretical works (Jaupart and Vergnolle, 1989; Proussevitch et al., 1993; Woods and Koyaguchi, 1993).

This work deals with a particular gas loss process from the shallow conduit system of Stromboli volcano. The present style of volcanic activity at Stromboli represents an example of persistent, volcanism protracting in the last 1500-years (Rosi et al., 2000). As

the geometry of its edifice has not appreciably changed since human records, Stromboli represents an interesting field case of permanent plumbing system operating very close to the steady-state condition. The volcanic activity is characterized by mild explosions of incandescent gas and bombs, with a variable amount of ash (i.e., Barberi et al., 1993). Between and during strombolian explosions, gas emission persists to feed a steady plume of gas. Gas emission has predominantly an origin in the degassing of magma with emission mainly concentrated in the open vents, as well as fumaroles and fractures on the inner and outer flanks of the crater structure (e.g., Allard et al., 1994; Finizola et al., 2002). Besides persistent degassing at Stromboli as in other active volcanoes is believed to occur at the equilibrium with the atmosphere (passive degassing, Figure 1, Andreas et al., 1991; Francis et al., 1993; Kazahaya et al., 1994), at Stromboli a second style of continuous degassing has been identified (Ripepe et al., 1996; Ripepe et al., 2007). Infrasonic (Ripepe and Gordeev, 1999; Ripepe et al., 1996) and thermal measurement (Harris and Ripepe, 2007) evidenced an intermittent (1-2 s time delay), low energy signals linked to the bursting of small hot gas pockets. These pressure perturbations operate alongside passive degassing and reveal that the persistent degassing at Stromboli occurs in overpressure condition. This work highlights how relevant this degassing mechanism is and demonstrates that degassing on a shallow magmatic column can be persistent and occurs at steady-state overpressurized conditions. This overpressurized degassing is here and after called *active degassing* to distinguish it from the passive counterpart.

The overpressure condition of this degassing mechanism requires the use of acoustic methods based on small aperture infrasonic array (Ripepe et al., 2004; Ripepe et al., 2007). This method has the advantage to return a precise quantification of the pressure and source location and an estimate the gas flux regime. Results have been used to define a schematic model of the shallow magmatic column at Stromboli. Finally, the analysis of infrasonic data collected by the permanent monitoring network (Ripepe et al., 2004) across the Stromboli 2007 effusive eruption and interpreted in terms of magma degassing (Marchetti et al., 2008; Aiuppa et al., 2008), allows the formulation of a possible dynamic model which well explains the fissure eruption at Stromboli, revealing the capability of infrasound to understand magma transport in the shallow feeding system.

2. Methodology

Infrasound on volcanoes

Volcanoes generate a large low-frequency acoustic energy (Richards, 1963). The acoustic frequency ranges from the audible sound (20-10000 Hz), produced by detonations, booming and whooshing listened during explosive activity, to frequencies below the audible bandwidth (0.1-20 Hz), called infrasound. In respect to the audible acoustic energy, low frequency portions have a lower attenuation, making infrasound the main target for volcano monitoring. In the latter decade, microphones sensitive to infrasonic frequencies have been employed in the vicinity of many active volcanoes (Table 2), allowing characterizing the infrasound wave-field produced by volcanic activity.

Infrasonic records represent the excess of pressure (ΔP) respect to the atmospheric pressure ($P_{\text{atm}} \sim 10^5$ Pa). Infrasound has been collected at volcanoes characterized by explosive activity and only few records are available for stronger eruption such as Plinian column. The excess pressure measured during this activity normally range between 10^1 and 10^2 Pa at distance between hundred to several thousands meters from the active vents, much smaller than the atmospheric pressure. In this case infrasound can be treated as a linear elastic wave, which allows simplify modelling of the source. At such distance moreover, infrasound generated by the source (0.5-10 Hz, Garcés and Mc Nutt, 1997; Hagerty et al., 2000; Johnson and Lees, 2000; Rowe et al., 2000) provide more direct information on the source dynamic compared to the seismic wave. The atmospheric Green's function does not significantly distort the waveform. In fact, at short distance, it can be assumed as homogeneous medium and scatter, attenuation and/or reflection effects are often negligible. Assuming a point source in a homogeneous medium, a compressional acoustic wave (atmosphere do not support shear waves) generated by an infinitesimal

pressure perturbation ΔP , propagates elastically according to linear equation of spherical waves:

$$\nabla^2(\Delta P) - \frac{1}{c^2} \cdot \frac{\partial^2}{\partial t^2}(\Delta P) = -F(t) \cdot \partial(r) \quad (1)$$

where $F(t)$ is the effective source force function.

Table 2. Summary of volcanoes where infrasound measurements and studies have been carried out. The amplitudes (Pa) are referred to 1 km of distance.

Volcano	Reference	Year	Pressure (Pa)
Arenal	<i>Hagerty et al., 2000</i>	1997	100
Volcán de Colima	<i>Unpublished</i>	2003	10
Erebus	<i>Rowe et al., 2000</i>	1997-98	200
Etna	<i>Marchetti et al., 2008</i>	2005	100
Fuego	<i>Johnson et al., 2004</i>	2003	100
Karimsky	<i>Johnson and Lees, 2000</i>	1997-99	10
Kilauea	<i>Garcés et al., 2003</i>	2002	0.2
Klyuchevskoi	<i>Firstov and Kravchenko, 1996</i>	1983, 87	25
Montserrat	<i>Ripepe et al., 2008</i>	2008	140
Sakurajima	<i>Garcés et al., 1999</i>	1986-88	40
Sangay	<i>Johnson et al., 2003</i>	1998	20
Santiaguito	<i>Johnson et al., 2004</i>	2003	2
Stromboli	<i>Johnson et al., 2004</i>	1996-2009	0.1-70
Unzen	<i>Yamasato, 1997</i>	1992	2
Villarica	<i>Johnson et al., 2004</i>	2002	20
Yasur	<i>Marchetti et al., 2008</i>	2008	100

The solution of this propagation equation can be written in the form:

$$4\pi r \Delta P = -F \left(t - \frac{r}{c} \right) \quad (2)$$

where r is the distance between source and receiver and c the sound speed, which can be computed as:

$$c = \sqrt{\frac{E}{\rho_a}} = \sqrt{\gamma RT} \quad (3)$$

where E is the bulk modulus (Pa), ρ_a the air density (kg/m^3), γ the heat capacity ratio, R the gas constant (287 J/kg/K), and T the temperature (K). At standard temperature and pressure the heat capacity ratio γ can be assumed as 1.4 and the sound speed c is directly proportional to the square root of the temperature (Ford, 1970). In the lower atmosphere and at temperature ranging from -10 to 40 °C, typical extreme conditions for many active volcanoes, acoustic waves velocity ranges between 325 and 355 m/s. Therefore at mitigated latitude such as Stromboli where ambient temperature is generally between 0-30 °C the velocity of sound can be reasonably considered as constant ($c=342$ m/s).

The most accepted models for the infrasound generation are i) the explosion of a gas bubble near the surface of the magma column (Vergnolle and Brandeis, 1996; Ripepe et al., 1996) and ii) the resonance of trapped waves in the magma body (Buckingham and Garces, 1996). In the latter model, the explosive source, embedded in, or at the top of the magma column, explains both the generation of long period, harmonic, seismicity (Chouet, 1985; Neuberg, 2000) and infrasound signal (Buckingham and Garces, 1996). Besides the ongoing debate, many researchers agree on the fact that on open conduit volcanoes the rapid release of gas with a certain of overpressure at the free surface is the main source of infrasound. Visual and video observation (Firstov and Kravchenko, 1996; Rowe et al., 2000; Johnson and Lees, 2000) evidence the generation of infrasound signals in relation with the emission of hot gas from active vents. In these volcanoes the strong damping of the shallow, bubbly rich (>70%), magma-gas mixture moreover, prevents the resonance effect

and the infrasound wave can be transmitted into the atmosphere only if the source is located in the shallow (< 10m) portion of the magmatic column (Marchetti et al., 2004). Infrasound records from such volcanoes revealed different and distinct signature, suggesting different degassing behaviours (Figure 2). Infrasound consists only in a single impulsive compression signal followed by a rarefaction (Figure 2a). These signals are related to strombolian explosions observed on many active, open vents volcanoes. In other cases, infrasound consists of a series of intermittent compressional impulses with different amplitude and time delay (Figure 2b). This style is indicative of sustained degassing observed during long-lasting volcanic phenomena such as lava fountains or pyroclastic flows (minutes to hours), or simple continuous degassing of a shallow magmatic column (month to years).

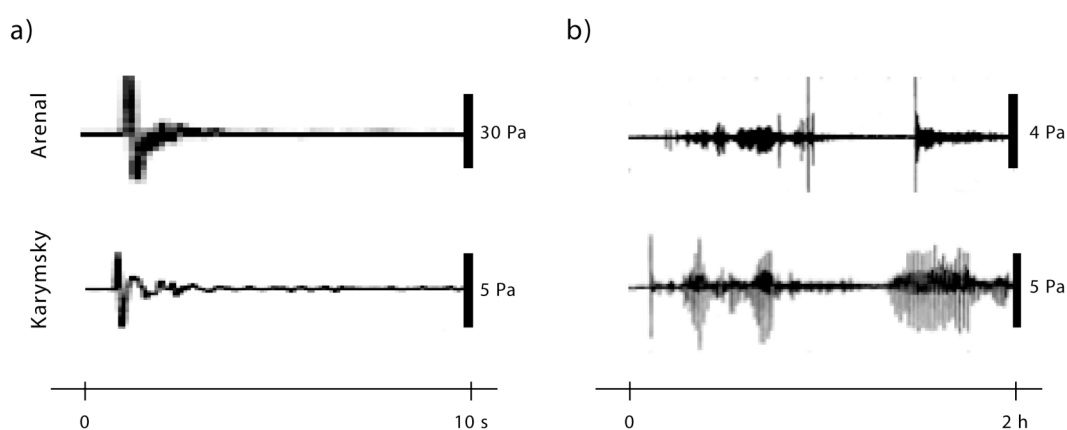


Figure 2. Example of infrasound records on volcanoes. a) Single impulsive compression followed by a rarefaction and b) repetitive, long lasting, impulses, at Arenal (Hagerty et al., 2000) and Karymsky (Johnson and Lees, 2000) volcanoes, respectively.

Hence, the infrasound analysis on active volcanoes represents a powerful tool to study the dynamics of a shallow magma degassing system. In particular, the use of small aperture infrasonic array is a valuable method for a precise location and characterization of the explosive activity on volcanoes. The coherence across a small aperture infrasonic array can be used to i) best discriminate signals from noise, and ii) to detect the back-azimuth direction of the infrasonic wave front (Ripepe and Marchetti, 2002, Garcés et al., 2003a) with a spatial resolution of only few degrees if employed in the near (<500) field (Ripepe and Marchetti, 2002). Their efficiency is limited only by strong winds, which cause a

decrease in the signal-to- noise ratio. However the ongoing research associated with the International Monitoring System (IMS) (Hedlin et al., 2002) is leading to an increase of the sensitivity of infrasonic arrays. Arrays deployed for the Comprehensive Nuclear-Test-Ban Treaty (CTBT) are able to track the trajectory of meteoric bolides (Evers and Haak, 2003) and the rupture propagation along faults (Olson et al., 2003) or to locate the source of oceanic surf (Garcés et al., 2003b). Infrasonic arrays are relatively inexpensive and easy to install. Their deployment does not require specific constraints, such as line of sight (e.g. radiometers, video cameras) or orientation of the sensors (e.g. seismometers, tiltmeters). The limited cost, the easy deployment and the high accuracy make small aperture infrasonic arrays an important tool in new volcano monitoring system.

Is by means of small aperture infrasonic array that the continuous degassing processes of the shallow magmatic column present at Stromboli is analysed in this work of thesis in terms of i) regime, ii) gas output and iii) source location and dynamics.

Small aperture infrasonic array at Stromboli

In March 2003 a permanent 5 element infrasonic array was deployed on the summit of Stromboli (Ripepe et al., 2004), at ~ 450 meters from the active craters and at a mean elevation of ~800 m (Figure 3).

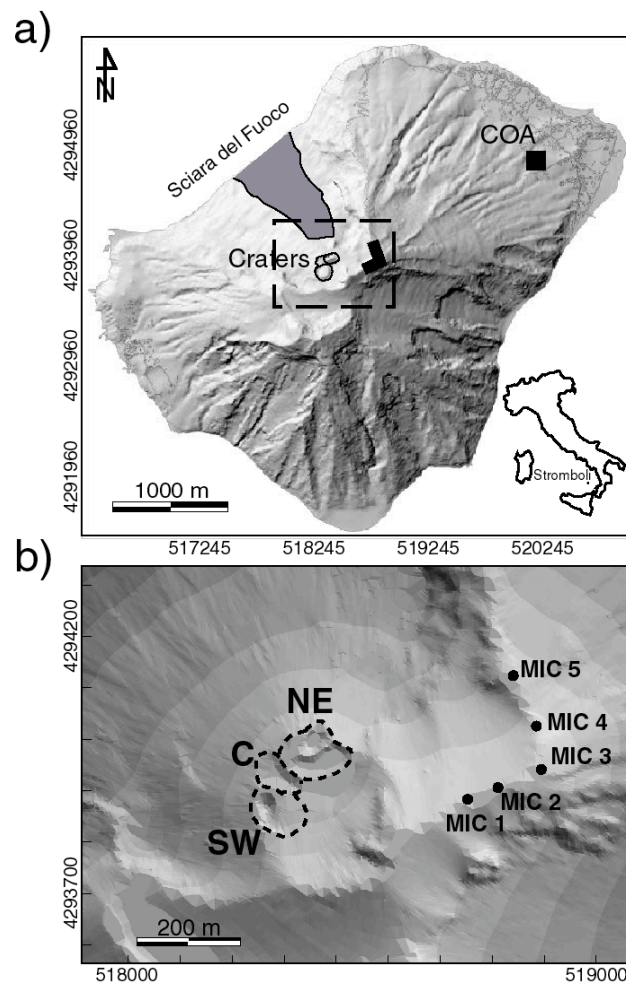


Figure 3. (a) The permanent infrasonic array (L-shaped area) positioned on the summit of Stromboli volcano at 450 m from the active craters. Digital data are radio transmitted to the monitoring center (square) organized by the Department of the Civil Defense of the Italian Ministry of the Interior in the village of Stromboli. The grey area represents the surface of the landslide, which occurred on 30 December 2002 at the onset of the eruption. (b) Detail of the summit area of Stromboli, showing the position of the five elements of the array (circles) with respect to the active craters.

The array consists on 5 pre-amplified electret condenser microphones, with a sensitivity of 50 mV/Pa, deployed in a L-shape configuration with an internal spacing of ~ 100 m. Position, geometry and aperture of the array have been designed i) to obtain the best azimuthal coverage of the different active craters, ii) to record coherent infrasonic waves in the 1-10 Hz frequency band, and iii) to easily discriminate between infrasonic onsets.

The 5 elements of the array are connected to the acquisition system by an optical fiber cable, placed ~ 50 cm deep in the ground. The use of optical fibre ensures the best signal-to-noise ratio (SNR) and reduces the risk of damages related to lightning. The signal recorded by the microphones is low-pass filtered below 20 Hz to enhance the infrasonic band and then is adapted to the optical fibre using a voltage-to-frequency converter operating at 10 KHz. This frequency-modulated signal drives a high-power solid-state laser, which is switched on only for 10 μ sec to reduce power requirements. Power at each element of the array (~ 0.1 W) is supplied using small 5 Watts solar panel. Before the digital acquisition, the frequency-modulated infrasonic signal is converted back to voltage by using a photo-diode receiver and is again low-pass filtered (< 20 Hz) to remove the electronic noise introduced by the frequency-to-voltage conversion. The signal is then converted to digital using a 16 bits converter working at 18.5 ms sampling rate and radio transmitted, at a frequency of ~ 1.2 GHz, to the recording centre located at ~ 2000 m of distance in the village of Stromboli. The array is working in this configuration since 2003 with no gaps.

The Electret Condenser Infrasonic Sensors

The infrasonic sensors used in our array are Horn EM9765 electret condenser microphones. The use of electret condenser microphone as infrasonic microphone was introduced for the first time in 1992 (Braun and Ripepe, 1993). At Stromboli since then many infrasonic sensors based on electret condenser microphone have been developed and are now widely used to monitor active volcanoes around the world (see Johnson et al., 2003 for a review).

Electret microphones are attractive because are inexpensive, robust, and have a low-power consumption. However, these cheap microphones have generally a flat response function in the audible band (from > 20 Hz to ~ 20 KHz) and thus are not specifically designed to operate in the infrasonic range (< 20 Hz). For this reason the calibration curve and the sensitivity below 20 Hz is generally unknown. This uncertainty in the response function makes the electret microphones unsuitable for a detailed waveform analysis without a detailed laboratory calibration.

We calibrate our electret condenser microphones using a MKS absolute differential pressure transducer, with a flat response function from DC to 50 Hz and a resolution of ~ 0.1 Pa. Calibration is achieved inducing a known pressure variation inside a sealed pipe gauge with internal diameter of 30 mm and length of 24 cm. A piston is installed at one end of the sealed pipe, while the electret microphone and the absolute differential pressure transducer are positioned at the other end. A step function causes a controlled movement of the piston inside the tube changing the volume of air inside the pipe and thus producing a known change of pressure. This change of pressure is measured both by the electret condenser microphone and by the MKS absolute differential pressure transducer (Figure 4). The last evaluates the pressure difference between the sealed pipe and a fixed reference volume of 20 cc of air at ambient pressure. This calibration shows that the response time of the pressure transducer is ~ 20 ms, much shorter than the one of the electret condenser microphone (~ 35 ms, in the specific case presented here). The response of the electret microphone to the step is used to calculate its complete transfer function. Microphone generally show a flat response in the frequency range 4-15 Hz (Figure 5), with sensitivity decreasing below -3dB for frequencies lower than 2.2 Hz and higher than 23 Hz, where

this high-frequency cut-off results from the electronic low-pass filter used as anti-aliasing filter to limit the audible band effects on the signal.

While the pressure transducer records the persistent overpressure, the electret condenser microphone gets back to initial value once pressure is stable again. The last evidences that the electret condenser microphone is recording the change in pressure rather than its absolute value.

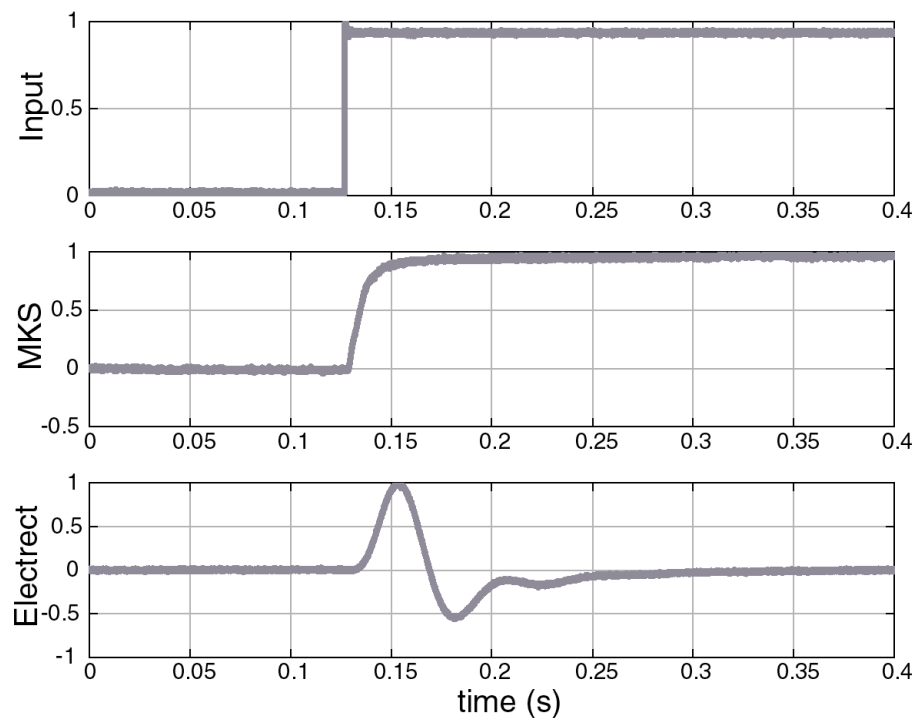


Figure 4. (a) Pressure step induced in the sealed pipe by the piston as recorded by the (b) absolute differential pressure transducer and (c) electret condenser microphone. Amplitudes have been normalized. The absolute pressure transducer is nicely following the pressure step, while the microphone has a longer response time (35 ms) and gets back to the initial values once the perturbation finishes and the pressure value is stable again. This calibration allows a precise estimation of the sensitivity for the electret condenser microphone (5.1 mV/Pa in the case presented here).

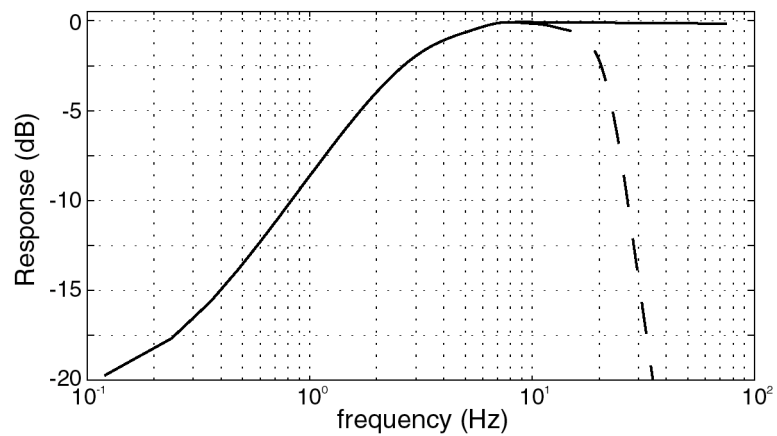


Figure 5. Transfer function of the electret condenser microphone. The microphone has a flat response for frequencies >3.5 Hz (solid line). Sensitivity decreases below -3 dB at frequencies <2.2 Hz because of the poor efficiency response of the electret condenser microphone in the low-frequency band. At frequencies >23 Hz, sensitivity decreases below -3 dB because of the four-pole, low-pass filter (dashed line) used to reduce the contamination of the audible sound in the infrasonic band.

Analysis of infrasonic data by means of array

In multi-vent or in complex crater systems a correct risk assessment depends on our ability to monitor the evolution in time and space of the activity at the different craters. This can be achieved by using the coherence properties of the infrasonic signals across the array. Generally, array techniques are based on the assumption of the propagation of a plane wavefront across the array, valid only if the aperture of the array is several times smaller than the distance from the source. In this geometrical conditions (Garcès et al, 2003a) array analysis is based on the Progressive Multi-Channel Correlation (PMCM) algorithm (Cansi, 1995) and can estimate the arrival incident azimuth and the propagation velocity across the array as a function of time and frequency content. Our array has an aperture (~ 400 m) comparable to the distance from the source (~ 450 m) and thus the assumption of a plane wavefront is not valid. For this reason we have developed a new algorithm for the automatic detection of coherent infrasonic signals in spherical wavefront conditions (Ripepe et al., 2007). The algorithm employed is based on a grid and/or line-searching procedure and aims to run with the minimum computing time on a single computer keeping the highest resolution and the best coverage of the crater terrace.

On a grid searching procedure, infrasonic source is searched over an area of 400×400 m equispaced every 10 meters and centred on the crater terrace at a fixed elevation (z_o) of 750 m a.s.l. (Figure 6a). For each node (x, y, z_o) we calculate theoretical infrasonic travel times ($\Delta t_i(x, y, z_o)$) at the different microphones (i) of the array, assuming spherical wave propagation and a mean sound speed (c_{air}) of 340 m/s in the atmosphere at 20°C and 900 m a.s.l:

$$\Delta t_i(x, y, z_o) = \left[(x - x_i)^2 + (y - y_i)^2 + (z_o - z_i)^2 \right]^{1/2} c_{air}^{-1} \quad (4)$$

where (x_i, y_i, z_i) are the coordinates of the i -th element of the array. Vertical position of the infrasonic source (z_o) is at this stage considered fixed at an elevation of 750 m. This latter assumption is speeding up the algorithm and it is supported by the numerical evidence, as

will be discussed later in the paper, that the position of the infrasonic source in the vertical plane is not changing in time.

According to equation 4, infrasonic signals recorded by the array are delayed by the corresponding theoretical travel time $\Delta t_i(x, y, z_o)$, and then the semblance $s_{ij}(x, y, z_o)$ among infrasound recorded at different couples of stations is calculated:

$$s_{ij}(x, y, z_o) = \frac{COV[P_i(t - \Delta t_i(x, y, z_o)), P_j(t - \Delta t_j(x, y, z_o))]}{\sigma[P_i(t - \Delta t_i(x, y, z_o))] \times \sigma[P_j(t - \Delta t_j(x, y, z_o))]} \quad (5)$$

where COV is the covariance and σ is the standard deviation of the infrasonic records ($P(t)$) at stations i and j of the array. Equation 5 is applied to all the possible permutations among signals recorded at the 5 elements of the array, providing for each node (x, y, z_o) of the searching line or grid a mean semblance $S(x, y, z_o)$:

$$S(x, y, z_o) = \frac{\sum_{i=1}^{N-1} \sum_{j=i+1}^N s_{ij}(x, y, z_o)}{\sum_{i=1}^{N-1} i} \quad (6)$$

where N represents the number of array elements ($N=5$). Values of $S > 0.6$ are assumed to be indicative of well-correlated signals. The source will be then located in the nodes, which according to the distribution of the mean semblance $S(x, y, z_o)$ have values higher than 0.6.

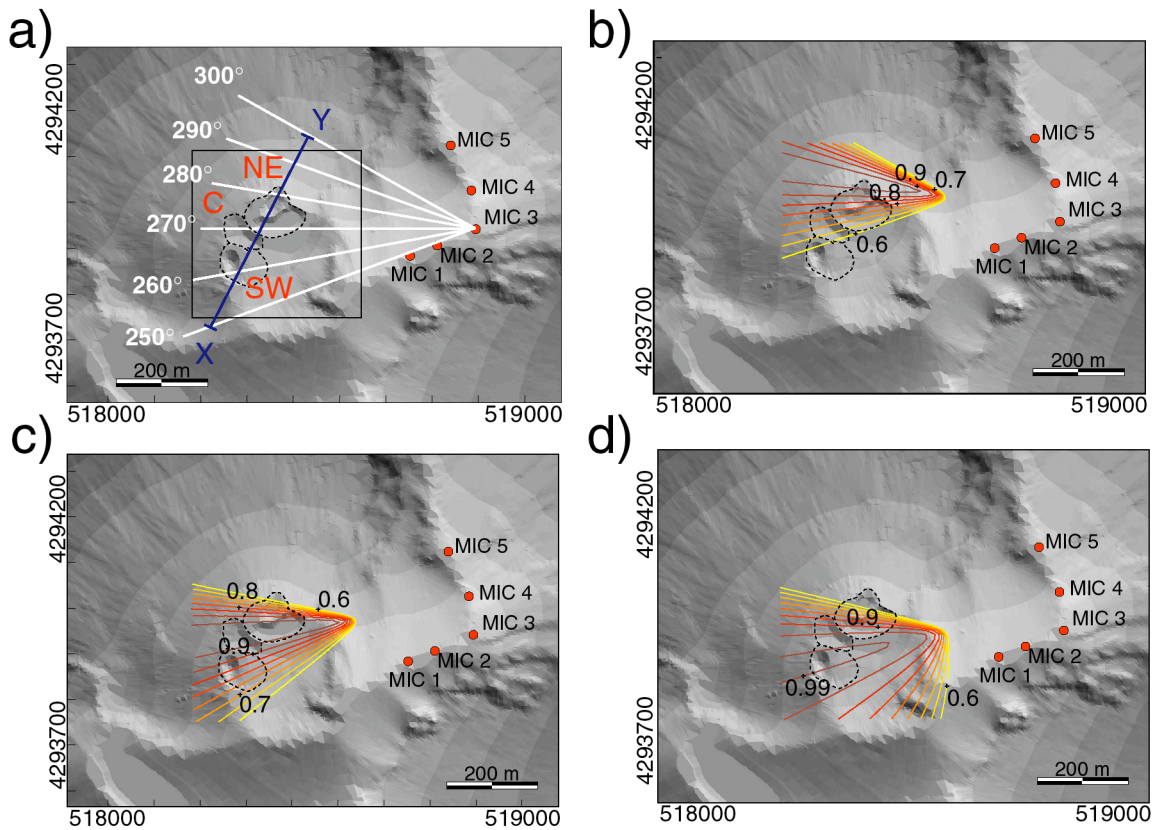


Figure 6. (a) Map of the summit of Stromboli volcano showing the position of the array with respect to craters and the position of the searching area used in the real-time location of the infrasonic source. The digital elevation map shown here is based on the morphology of the crater terrace before the Stromboli volcano's December 2002 eruption and landslide. The grid (square) extends over an area of 400 x 400 m with an internal spacing of 10 m centred on the crater terrace. The position and dimension of the grid allow us to investigate all of the possible infrasonic sources on the crater terrace, and the spacing (10 m) allows us a good discrimination between different vents. The line (X-Y) across the searching grid gives the position of the vertical plane used for searching for the source elevation (see Figure 6), while the white lines converging to the central microphone (MIC 3) represent the angles considered in the back azimuth searching procedure (Figure 9). Examples of source location for acoustic signals associated with (b) an explosion at the NE crater, (c) degassing at the central crater, and (d) an explosion at the SW crater. Contour lines represent the mean semblance $S(x, y, z_0)$ distribution on the grid and indicate the most probable direction of the infrasonic wavefront.

Efficiency of the infrasonic array

Atmospheric conditions, such as humidity, temperature and atmospheric pressure, have a direct influence on the sound speed. For an ideal gas sound velocity (c) is given by:

$$c = \sqrt{\frac{\gamma RT}{M}}, \quad (7)$$

where γ is the adiabatic constant of the gas, R is the universal gas constant (8.314 J/mol K), M is the molecular mass and T is the temperature (°K) of the gas. According to equation (7) and to the perfect gas law, sound speed increases with pressure and temperature conditions in the atmosphere. A detailed analysis of sound speed as a function of ambient conditions (Cramer, 1993) reveals that at the Stromboli's latitude and for close distance from the source (~400 m), atmospheric conditions have a small influence on the change in sound speed, while they are critical in terms of reducing the efficiency of the instruments.

Humidity may induce a distortion in the transfer function of the electret condenser microphone while wind has a double effect, as it can change sound speed of the wave propagation and it represents a major source of noise. While the former effect of wind simply results in a variation of the effective sound speed (Garcès et al., 1998; de Groot-Hedlin, 2005), wind blowing on the microphone can induce local changes of pressure as large as >100 Pa, higher than the infrasonic signal produced by the explosion. Volcanoes are generally hostile environments highly wind exposed. Wind reduces the signal-to-noise ratio and it represents the only perturbation able to reduce the efficiency of the array in locating acoustic activity on volcanoes.

We have reduced the effect of wind and humidity on the array by: 1) wrapping the electret microphones in a foam, 2) shielding the microphones in PVC boxes, and 3) partially burying them underground. This combination of "infrasonic" foam and "transparent" PVC boxes has turned to be a good solution to reduce wind noise and to prevent humidity effect on the microphone. Signal-to-noise ratio (SNR) on each of the elements of the array remains high and this results in high values of the semblance across the array.

When SNR decreases, the infrasonic array will fail to locate the source, leading to a misinterpretation of the explosive level of the activity at the craters. For this reason, a proper infrasonic monitoring has to be associated with a real-time monitoring of the atmospheric parameters, including wind speed and direction. The semblance analysis on the infrasonic array over one month (January 2004) characterized by relative strong winds reveals the efficiency of source location (Figure 7).

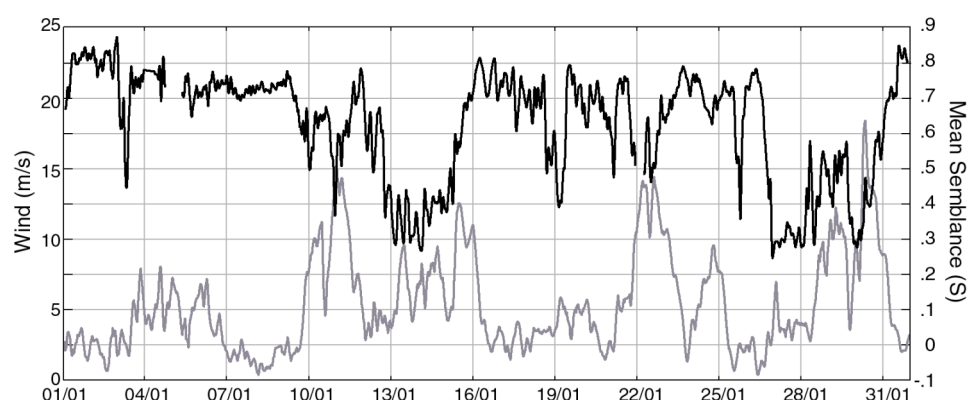


Figure 7. Wind influence on the array efficiency. We compare semblance (dashed line) with the wind speed (gray line) measured in January 2004. The wind speed records help us to understand when the calculated low (<0.6) values of semblance are related to a reduced array efficiency by the wind or to a decrease of the volcano infrasonic activity. Only a wind speed >10 m/s (11, 15, 22, and 29 – 30 January) is responsible for low semblance values, while all of the other episodes have to be related to a decrease of the volcano acoustic activity.

The mean semblance ($S(x,y,z_o)$) among the array is lost only for wind speed larger than 20 m/s, while the array is generally locating infrasonic sources also with wind speed of ~ 10 m/s. This efficiency in locating the source also with strong wind is possible because wind has only a local effect on the array. Wind will not generally blow with the same intensity on all the microphones at once and accordingly low semblance ($s_{ij}(x,y,z_o)$) between channels with low SNR (Figure 8) will only partly affect the source location, leading to a small decrease of the final value of mean semblance. This explains why the infrasonic array is able to locate the source also when wind blows at speed over 10 m/s (Figure 7). Nevertheless, wind speed and direction should be carefully monitored to help understanding if an apparent reduction of infrasonic coherence is due to strong wind, or to a period of low activity.

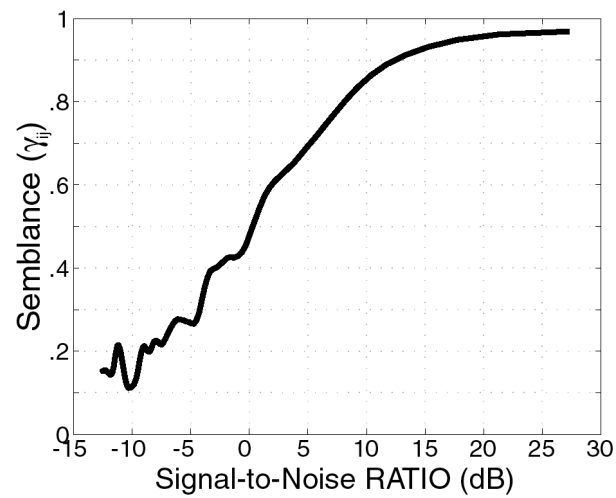


Figure 8. Semblance (γ_{ij}) calculated according to equation (5) between two infrasonic sensors, where one of them was contaminated by adding white noise with Gaussian amplitude distribution to simulate the local effect of the wind. The semblance also remains high (>0.5) when noise amplitude is equivalent to signal amplitude (SNR = 0 dB). Wind has a small effect on source location also with small-aperture arrays operating in windy and hostile environments such as volcanoes.

3. Infrasonic analysis of active degassing at Stromboli

The permanent gas plume above the volcano reflects the presence of continuous gas discharge and strongly indicates a continuous new supply of magma from depth. Gas discharge from summit vents and/or fumarolic field as well as the periodic explosive release of gas, represent the main degassing processes that feed the plume. The persistent gas discharge occurs at the equilibrium with the atmospheric pressure, while a certain degree of overpressure is necessary when the release of gas takes place in the explosive way. In the latter case, the infrasonic record represents the best way to measure the overpressurized gas discharge and analyze its dynamics.

Infrasonic explosions and puffing

Explosive activity at Stromboli is generally explained as the result of large gas slugs that, reaching the uppermost portion of the conduit, explode when their overpressure is no more compensated by the external pressure. This gas bursting of the magma column generates infrasonic transients (Ripepe et al., 1996; Vergnolle et al., 1996) (Figure 9a). Two major clusters of infrasound may be identified at Stromboli, reflecting the two end members of the explosive activity typically observed (Ripepe et al., 1993; Ripepe and Marchetti, 2002). Short infrasonic pulses (2-5 s) of high amplitude (up to 2 bar at the source) are commonly recorded during cannon-like explosions mainly observed in last ten years at the NE crater, while longer-lasting (10-20 sec) small amplitude (~1 bar at the source) transients are produced by the gas and ash emissions from the SW crater (Ripepe and Marchetti, 2002). The infrasonic records evidence the presence of a second type of signal, which consists of intermittent infrasonic pulses (Figure 9b). Degassing of a magmatic system is generally understood as a quasi-steady (Allard et al., 1994) “non-explosive” passive mechanism, which is active when the slow exsolution process allows the continuous pressure compensation of the gas rising through the magma column. In contrast, infrasound indicates that degassing can occur also in over-pressurized condition, associated to the

bursting of small gas pockets at the magma free-surface (Figure 9b). This intermittent release of gas induces in the atmosphere small ($< 0.1 \times 10^5$ Pa at the source) infrasonic pulses (Ripepe and Gordeev, 1999) and occurs almost regularly every ~ 1 -2 s (Figure 9b).

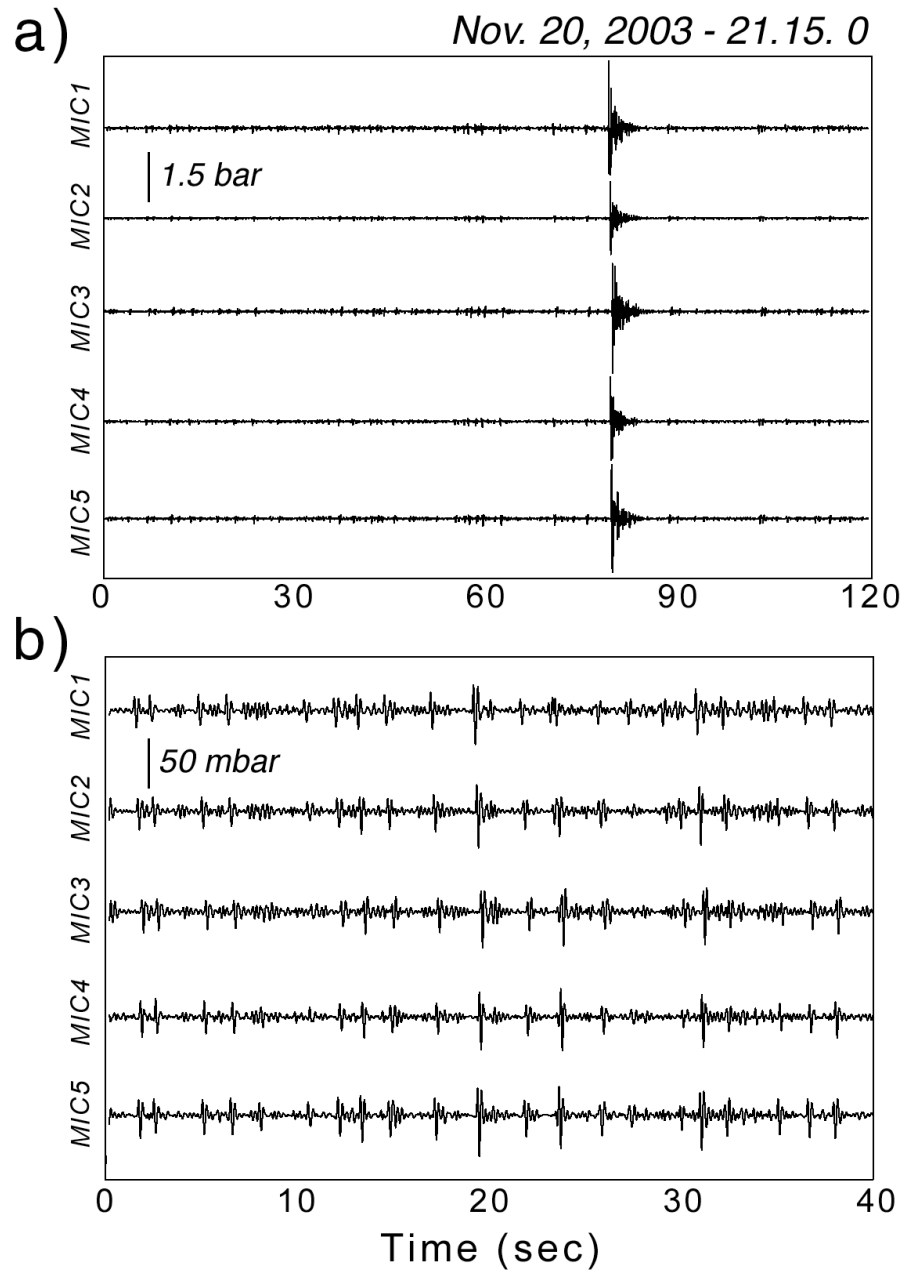


Figure 9. (a) Two-minute-long sample of coherent infrasonic data recorded by the five elements of the array showing intermittent degassing and one explosive event. (b) Detail of small-amplitude infrasonic transients repeating at 2-s time intervals. The small-amplitude infrasonic pulses in Figure 1b are related to the bursting of small gas bubbles on top of the magma column.

Detection of intermittent infrasonic pulses

Explosive activity and puffing are both generating infrasonic waves, which are detected by the array as a coherent signal. The permanent array operating at Stromboli provides the location of the source and the quantitative information on both phenomena, indicating over-pressure and occurrence of the transients, by which a detailed description of the infrasonic activity is available.

In order to extract infrasonic pulses, the searching analysis (equations (2) and (3)) is applied on windowed infrasonic array records. The length of the window and the shift of analysis have been opportunely selected to correctly analyse an intermittent signal like the infrasonic puffing (Figure 9b). In general, the selection of the windows parameters mainly depend on the maximum delays between the 5 signals of the array, duration of each pulse and their recurrence time.

Looking at the puffing records, however, they reveal that the length of pulses (< 0.6 sec) is less than the recurrence time (1-2 seconds), such as no overlap between consecutive pulses is observable on a single trace (Figure 9b). In this case the possibility to analyze each transient on an individual window, depends mainly on the maximum delay in the array, which in turn depends on the geometrical ratios between each element of the array and the source (Figure 10). A recurrence time larger than the maximum delays of signals in fact determines the possibility of more than one signal on the window, making difficult the analysis. Assuming a spherical sound wave, with a velocity ranging from 340 to 350 m/s and propagating from the 41 source points of the line-searching procedure (Figure 10), the theoretical delays on the Stromboli's array is ranging from 0.28 seconds to a maximum value of 0.5 seconds for a source located in the SW active vents (Figure 11). The 0.6 s value has to be considered as the lower bound for the window length in order to ensure the presence of all five transients on the window of analysis.

Based on these considerations, a 1-second-long window and 0.5 second shift has been used for determine correct information on infrasonic puffing activity at Stromboli. The 1-second-long window ensures the presence of a single pulse on each record of the array, while reduces the possibility to analyze multiple events on the same window. The short length of the shift, guarantees that at least once the window passes over each pulse.

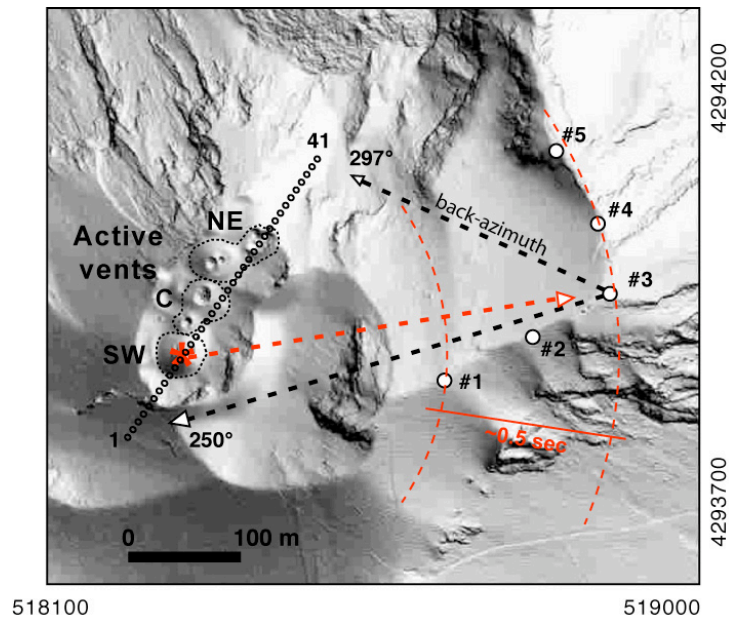


Figure 10. Map of the summit of Stromboli volcano (Oct, 2006) showing the 5-element infrasonic array, the active vents (SW, C and NE), and the position of the 41 theoretical sources points (10 m equi-spaced) used for the line searching procedure. Red and black arrows indicate the direction of propagation of sound from source and the relative back-azimuth angle returned by the analysis in relation to a source located on the SW vent, respectively.

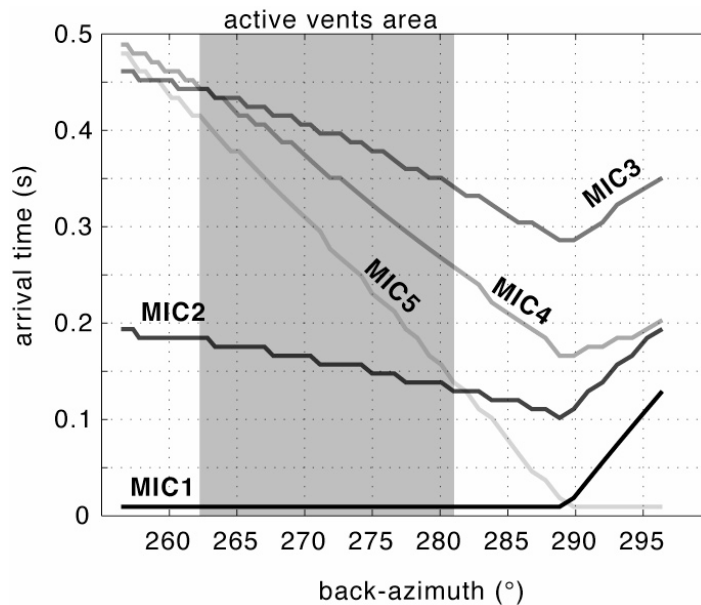


Figure 11. Distribution of the arrival time on the array in respect to a series of sources impinging the array with a direction of propagation (or back-azimuth) between 255 and $\sim 300^\circ$ N relative to the central (MIC3) element of the array (Figure 10). A 340 m/s sound velocity and spherical wave propagation were assumed. Within the sector of active vents (grey area, $262\text{--}281^\circ$ N), the maximum time delay within the array is ~ 0.5 second relative to a source located at SW (Figure 10) vents (261° N).

However, multiple detections of the same signal are possible. As described later, though the puff length and intermittency allow minimizing the latter effects. The short length of shift (0.45 s) requires a large number of computations to analyze in detail the puffing activity. Therefore, a simpler line-search on 41 nodes (Figure 10) has been adopted instead of that for a grid of 40x40 nodes of Figure 6. In this case the time required by a single personal computer with 2GHz clock to analyze a 1-hour set of data with a 1-second window and 0.5 second shift is ~ 3500 seconds. For the real-time processing of infrasound activity at Stromboli, this run-time is too large. In this case in fact, to reduce this run-time and to obtain a suitable speed the windowing has been reduced by a factor 8 (5-second-long windows shifted by 4 seconds), but averaged results can influence a parameter such as time delays.

On Figure 12 are shown the results of the line searching procedure carried out over 30-second-long signals during typical infrasonic puffing activity (Figure 12a). The searching analysis (equations (2) and (3)) is applied to the 1-second-long window shifted by 0.5 s. In the example, the selected window (Figure 12b) evidences the presence of coherent signal over the 5 (#1-5) records. For each window the #2-4 traces (Figure 12b) are shifted with respect to the #1 trace for a set of 4 times for each of the 41 nodes, resulting from the difference between the theoretical travel time at the 5 elements for the 41 source nodes (Figure 10). For each node the coherence is then calculated (equations (3)), giving the distribution along the line crossing the active vents (Figure 12c). This coherence analysis needs of a threshold value of semblance, which has been adopted in order to discriminate signal from noise. In this case the threshold has been fixed at 60% of semblance (Figure 12c, dotted horizontal line). When the maximum value of the coherence distribution exceeds the threshold, the analysis gives back 4 information (Figure 12, red circles) namely, the absolute time of the first positive amplitude t (referred to the #1 trace), the overpressure ΔP (Pa), the maximum coherence C_{max} (%), and the corresponding direction of propagation or *back-azimuth* ($^{\circ}$ N). In the example, the 1-second-long time series of infrasonic array contains a signal ($C_{max} > 60\%$) with ~ 2.5 Pa of overpressure propagating across the array, at a sound velocity of 340 m/s, with a back-azimuth direction of 284° N.

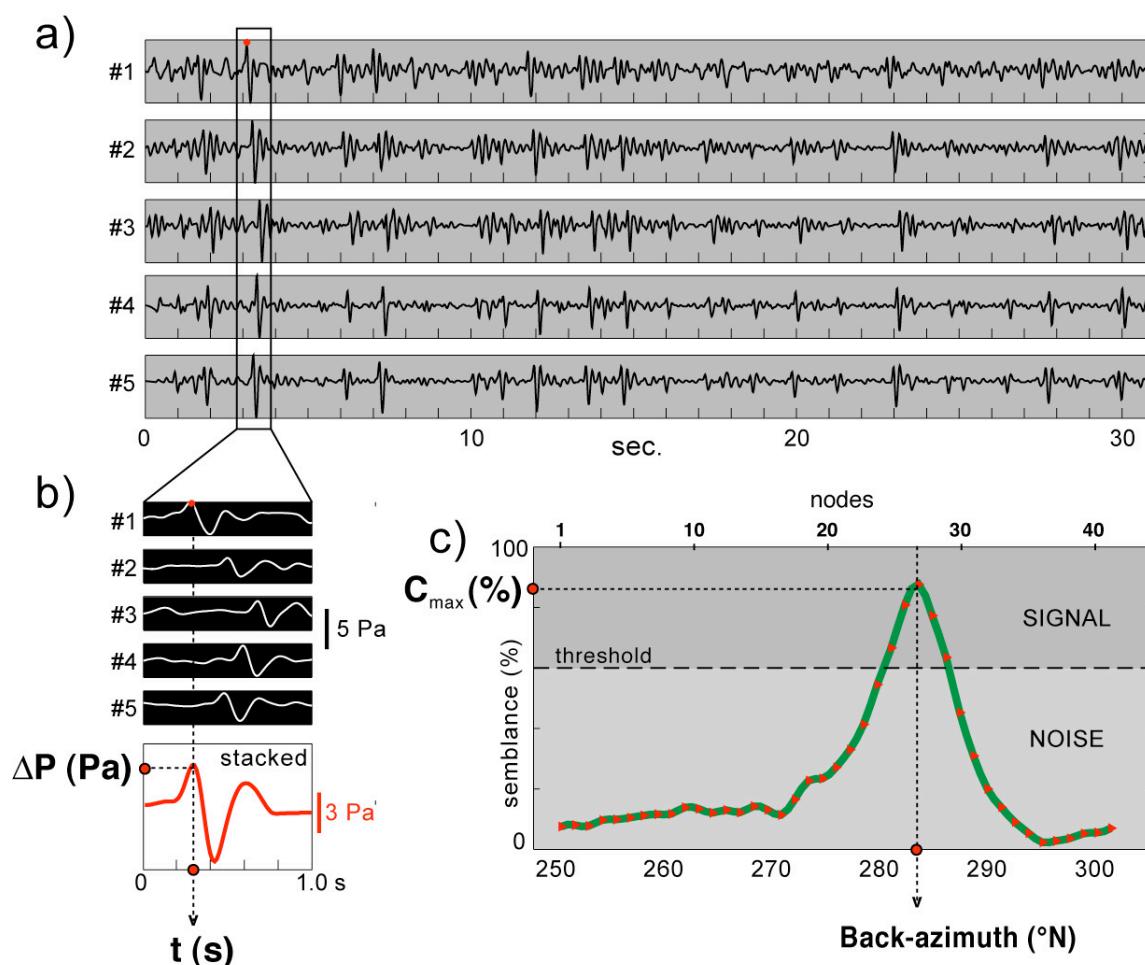


Figure 12. One step of the line searching procedure used for the analysis of infrasonic puffing at Stromboli. a) 30-second-long traces of 5-elements (#1-5) infrasonic array during mild puffing activity, with the rectangle indicating the analyzed window. b) Window of traces (#1-5) and stacked waveform resulting from the sum of the shifted 5 traces. Each of the #2-4 traces is shifted with respect to the #1 trace of an amount corresponding to the theoretical travel times for each of the 41 source points (Figure 10). c) Distribution of the coherence between the shifted traces over the 41 source points. In this example the maximum coherence ($\sim 87\%$) is obtained for a source node 27, where a threshold of 60% is assumed to discriminate signal from noise. Red circles indicate the values of the 4 output parameters extracted by the line-searching procedure: 1) occurrence time (t), 2) overpressure (ΔP), 3) maximum coherence (C_{max}), and 4) back-azimuth. The threshold line indicates the minimum value of coherence to discriminate signal from noise.

On Figure 13 a sample of a 24-hour-long infrasonic activity in term of overpressure, back-azimuth and semblance is shown. Assuming the sensor #3 (Figure 10) as the centroid of the array, the position of the explosive vent is searched between 250° N and 300° N (Figure 10) at intervals of 0.5° , which at the distance of ~ 450 m are equivalent to a horizontal sampling of ~ 4 meters, small enough to discriminate activity at the three main summit vents (SW, C and NE). The analysis revealed both puffing and explosive transients.

Pressure (Figure 13a) and back-azimuthgrams (Figure 13b) of the puffing activity are shown as continuous, low amplitude (< 10 Pa) coherent ($>70\%$) signals with stable direction of $\sim 278^\circ\text{N}$, corresponding to the North-East (NE) vents, while isolated high amplitude (15-70 Pa) spikes with high semblance reflect the explosive activity at the South-West (SW) and Central (C) vents, the latter increasing since 20:00 GMT.

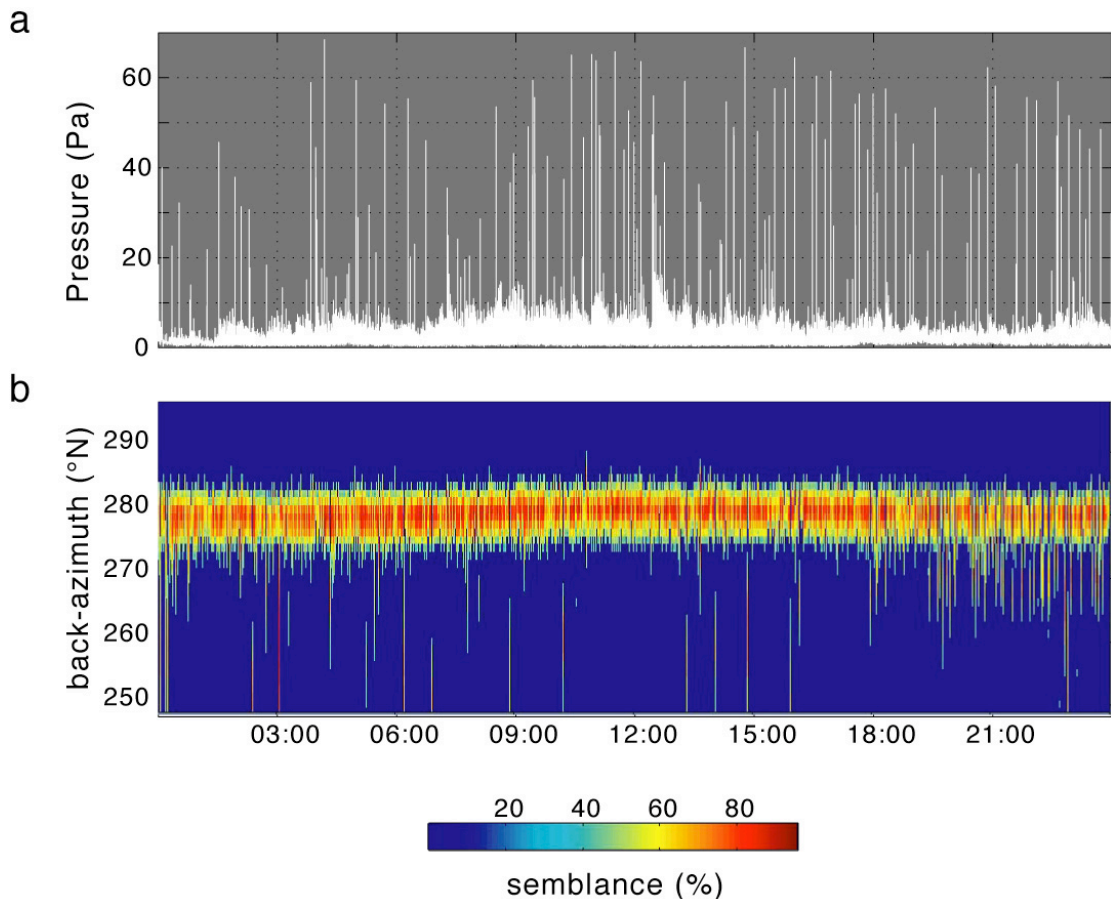


Figure 13. Results of a line-searching analysis on the infrasonic array data during one day of typical strombolian activity. a) Trend of the infrasonic amplitudes (Pa), and b) trend of the back-azimuth ($^\circ\text{N}$). The explosions appear as isolated, high amplitude (15-70 Pa), spikes either in a) and b), whereas the background small (1-10 Pa) amplitudes (a) with high values ($\sim 80\%$) of semblance for $\sim 279^\circ\text{N}$ of back-azimuth (b) reflect the persistent infrasonic activity composed of small-amplitude pulses repeating at intervals of a few seconds, called *infrasonic puffing*. The latter phenomena is the expression of the persistent degassing of the shallow magmatic column at Stromboli, called *active degassing*, and represents the target of this work. Colour bar represents the mean semblance (equation (6)) calculated on 1-second-long windows shifted every 0.5 s.

Parameters for active degassing derived from infrasonic data

The infrasonic array analysis yields parameters describing the intermittent puffing process as function of the recurrence time (∂t , sec.), amplitude (ΔP , Pa) and position (back-azimuth) of the source. The occurrence of small transients, such as the infrasonic puffing, at high rate (Figure 9b) must reflect the dynamics of an intermittent process. In this case, the measured excess pressure ΔP (Pa) should in some way reflect the intermittent pressure perturbation regime on the shallow magmatic column.

Relative to the seismic data, the analysis of infrasonic signal can more directly reflect the physical processes of the magmatic source, being the acoustic wave propagation in the atmosphere less distorted by scatter, attenuation and reflection effects. Given that a linear approximation is suitable for infrasound, in particular for the infinitesimal pressure perturbations of puffing ($P_{atm} - P_{pulse} < 0.1$ bar), the analysis of infrasonic puffing waveform has been carried out in this work in order to estimate the order of magnitude of gas mass flux during each single puff. The presence of a permanent infrasonic array at Stromboli and the short recurrence time of puffing pulses (1-2 sec.) have generated a large data set of transients per day (~ 40.000), which has been used to estimate the averaged mass flux for this continuous process.

Finally, the array allows precise location of the source. On active volcanoes with multiple active vents as Stromboli, location analysis revealed an important method to better characterize the phenomena.

The active degassing regime

The semblance analysis on 1-second-long window (Figure 12) allows a detailed description of the intermittent process in term of time delay between two successive puff. The small amplitude of the signals (1-10 Pa) and the short time delay between pulses (1-2 s) require some consideration for a correct analysis of the intermittent regime. Array analysis warrants a high efficiency to detect the real intermittence and/or the amplitude distribution. Variability in the response function of electrets condenser microphones, due for example to the extended exposition to variable temperature and humidity, should be minimized. These external variables can influence the results of a long time period analysis. However, the dataset should be longer enough to include large variation of amplitude and to give a statistical sustain to the analysis itself. In order to minimize the effect of wind activity and deterioration of the sensors, an ad-hoc, 7-days-long, period of variable infrasonic activity has been selected for the statistical, detailed analysis of infrasonic puffing regime (Figure 14).

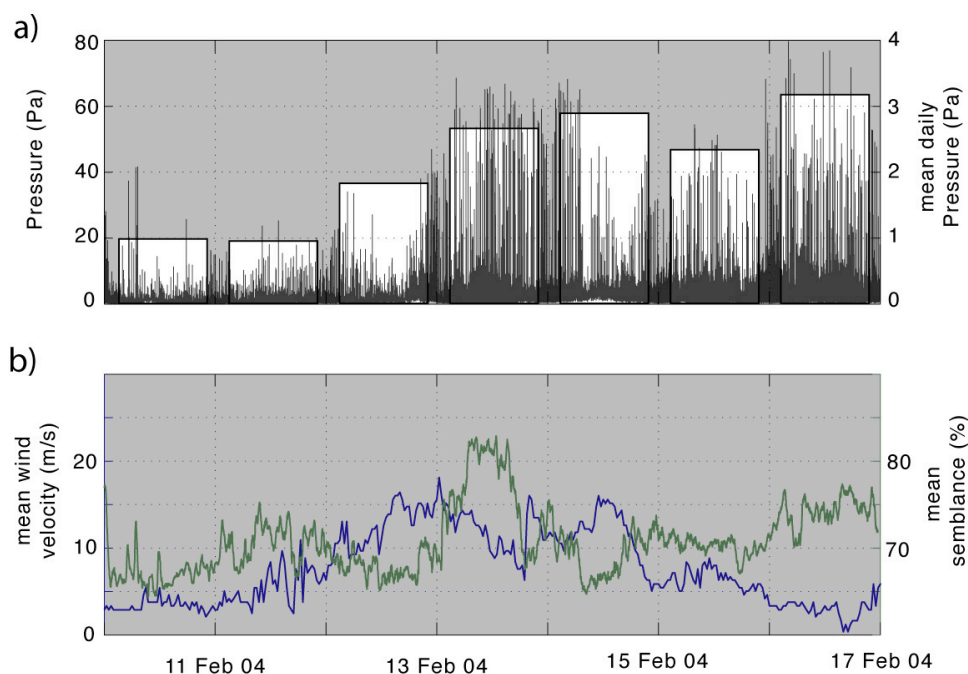


Figure 14. 7-days-long (February, 10-16 2004) of infrasonic and wind activity at Stromboli in term of a) amplitude (Pa), b) mean coherence across the array (black line) and wind velocity (white bars). This phase has been selected as it showed i) a wider variation in amplitude, ii) and a particularly high signal to noise ratio and mean to low wind activity.

Figure 14a (black lines) shows the trend of the amplitudes of the infrasonic signals detected by the array using the short windowing analysis, where both puffing (background amplitudes) and explosions (spikes amplitudes) transients are included. In order to enhance the main amplitude variations of puffing, the daily average is plotted with white bars in Figure 14a. As the recurrence time of puffing transients is 1-2 s, such an average is sufficient to represent the mean amplitude sustained process. Daily amplitude during the selected period varies from ~ 1 to 3.5 Pa, comprised within the main variation of the amplitude observed during the 2003-2006 time span (see Figure 26, bars). The mean semblance (equation (3)) across the array during that period (Figure 14b, black line), is on average high ($> 65\%$), evidencing a general high signal to noise ratio. The wind speed (Figure 14b, white line), which represents the main source of infrasonic noise, was generally low (< 15 m/s), providing a quite high efficiency of the array (Ripepe et al., 2004). Even if medium to high values (10-16 m/s) of wind were recorded, the wind generally will not blow with the same intensity on all the microphones at once, producing only a small decrease on the mean semblance. Wind during the selected period hence, should not significantly affect the analysis.

During this period, about 40.000 infrasonic events were identified. As expected, the short 0.5 second shift generates $\sim 6\%$ of data overlap, which have been removed from the dataset. Almost 34% of the extracted infrasonic signals, moreover, have a time delay less than 0.4 seconds. This family of events represents the coherent coda of the puffing and explosion signals. The high recurrence of this class of events in fact, will generate an artificial peak in the time delays distribution, which is not desired. The resulting number of infrasonic events consists of ~ 25.000 events during 7-days of activity, indicating approximately one events every ~ 2.4 seconds. The distribution of the time delays in the 0.4 and 10 seconds range shows an asymmetric distribution with a mode, mean and median of 1.3, 1.8 and 1.5 seconds, respectively, and a standard deviation of $\sim 50\%$ (Figure 15), reflecting a sustained, stationary volcanic process.

A regularly spaced infrasonic pulse has also been observed on other volcanoes; at Karimsky volcano (Kamchatka, Lees et al., 2004), the time delays between pulses were very stable (std $< 10\%$, Figure 16). These sequences of quasi-periodic pulses following the

explosive events and lasting only 30-60 seconds, called *chugging*, evidence direct relation between time interval and amplitude of chugs.

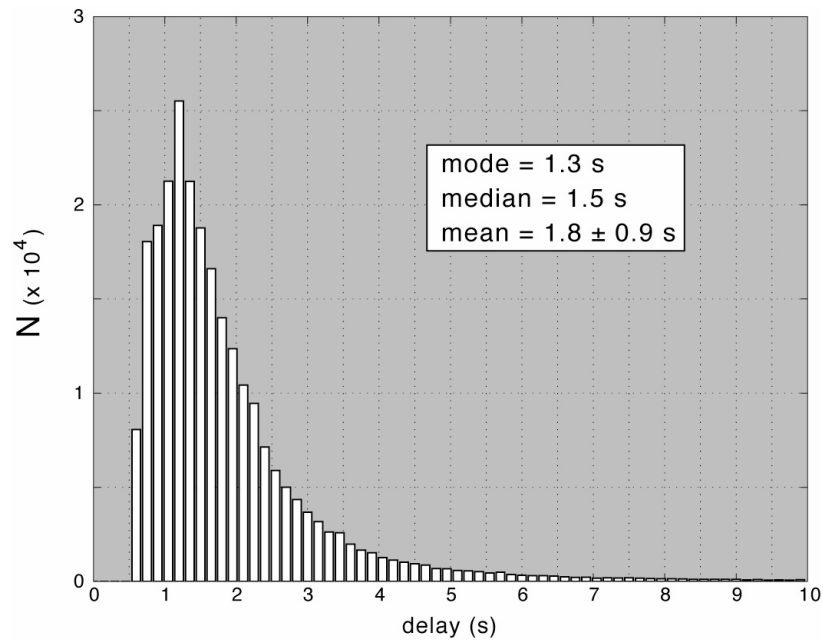


Figure 15. Frequency distribution of the time delays between successive infrasonic events during the February 10-16, 2004, in the range 0.6-10 seconds. The 2.5×10^5 events forming the dataset indicate continuous (~ 2.4 s of mean delay) puffing activity acting during the selected period. The most recurrent time delay is 1.3 seconds, the mean and median are 1.8 and 1.5 seconds, respectively, and the standard deviation is $\sim 50\%$.

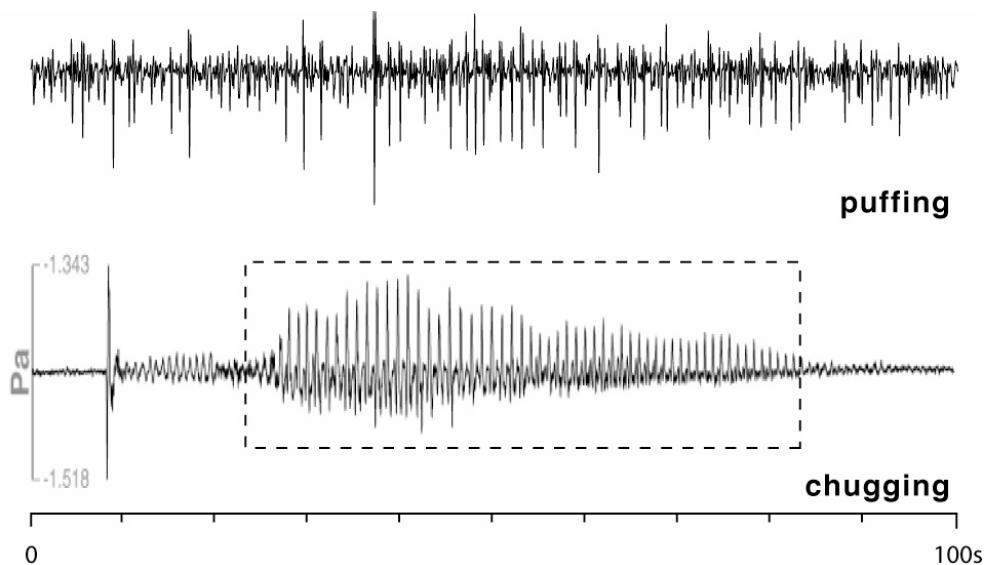


Figure 16. 100-second-long comparison of infrasonic puffing activity at Stromboli and infrasonic record of a chugging phase (dashed rectangle) at Karimnisky volcano (from Lees et al., 2004).

Based on these observations the authors invoke a process where the storage of energy in the system between pulses controls the time and the amplitude of the chugs. That is, the longer the delay the higher the energy is stored. At Stromboli, however, infrasonic pulses repeat irregularly on short time scale (10 s to 1 minute), indicating a repetitive process that is not time controlled. In order to verify if some link in the puffing regime exists at longer time scale, we analyzed the distribution of the time delay over 1-hour-long windows with 0.5 hours of shift (Figure 17). At hourly time scale, the mean intermittency shows limited variation (1.2-4.5 seconds) in the 0.8-4 Pa amplitude range which reflects the large variations of puffing activity at Stromboli.

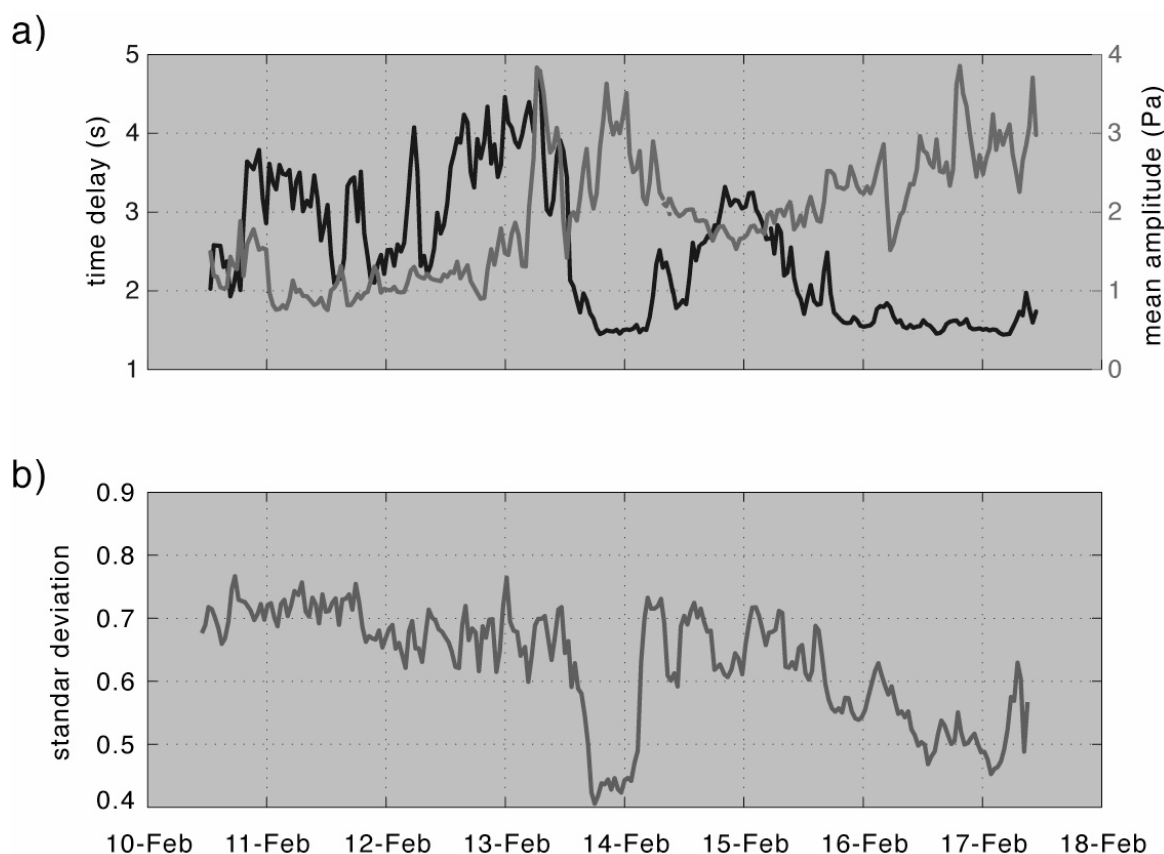


Figure 17. a) 7-days-long trends of the a) 1-hour-long average of mean delay (black line) and mean amplitude (grey line) of infrasonic pulses, and b) mean standard deviation. The mean time delay varies within a short range (1.5-4.5 seconds) over the 0.8-4 Pa of amplitude. A bimodal behaviour is observable, as the shorter the mean delay the higher the mean energy released.

Averaged longer time delays are observed during low amplitude pulsation (10 to 14 Feb, Figure 17), which shifts to shorter values in relation to the increment of mean amplitude

(14 to 16 Feb, Figure 17), following an inverse relation (Figure 18). Linear inverse relation is observed within the short range of time delay (1.2-2.5 s), and is lost for very low mean amplitude (< 1 Pa). The large increment of the mean amplitude of the phenomena, is characterized by a general decreasing of the, evenly high, standard deviation (from 0.4 to 0.7), indicating that during higher energetic phases the intermittence becomes relatively more stable.

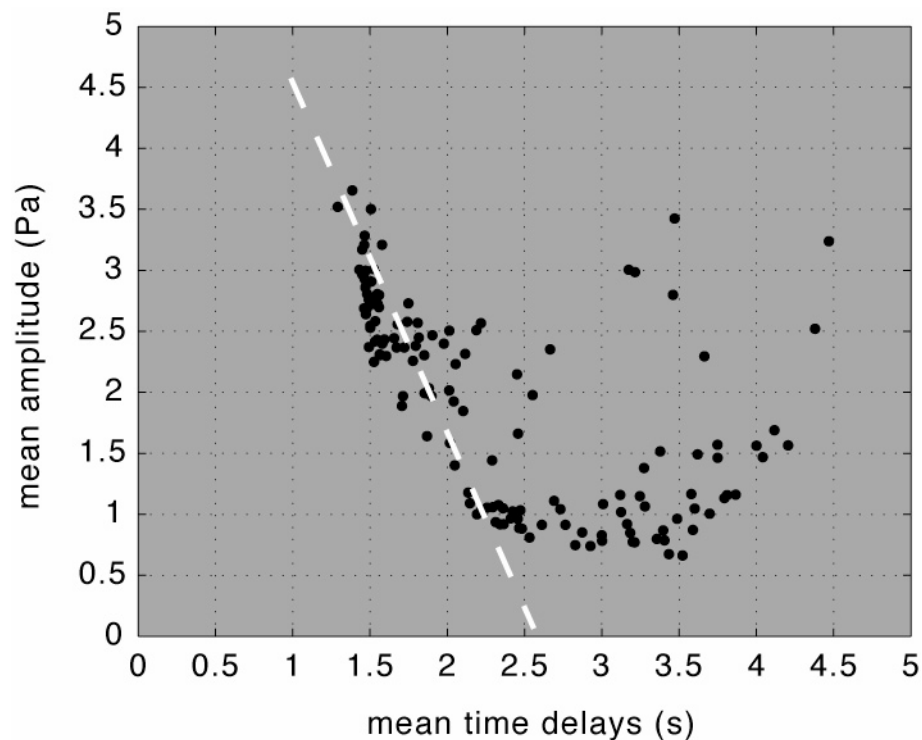


Figure 18. Relation between the mean time delay and amplitude of infrasonic pulses within 1-hour-long windows and 30 minutes of shift. An inverse relation is observable between 1.4 and 2.5 second, while for longer delay the relation is scattered.

Inverse relation between the energy and pulsation of the system is observed on many processes driven by the flux of energy, for example the increase of the round per minute carried out by a car motor at increasing fuel flux into the combustion. In particular, the fluid-dynamics of two-phase (air-water) system in tubes has been extensively studied in laboratory for industrial purposes.

Insight on source and mass outflow

A single infrasonic transient (here and after puffing) recorded at ~ 500 m from the source consists of small (1-10 Pa) pressure signal with positive onset followed by a negative oscillation and a short lasting, strong attenuated, coda. The entire transient lasts < 1 second (Figure 19). The comparison of ~ 1200 puffing events isolated by means of coherence analysis on array show that the shape and duration of such signal is quite stable for a wide (1-10 Pa) amplitudes range (Figure 19), resulting in a stable frequency content between 3 and 5 Hz. Only smoothly differences in waveform are founded at different position (#5, Figure 10 and Figure 19). The simple and stable character of puffing signals evidences a impulsive, non-destructive source generating small pressure perturbation at the origin of puffing activity recorded at Stromboli volcano.

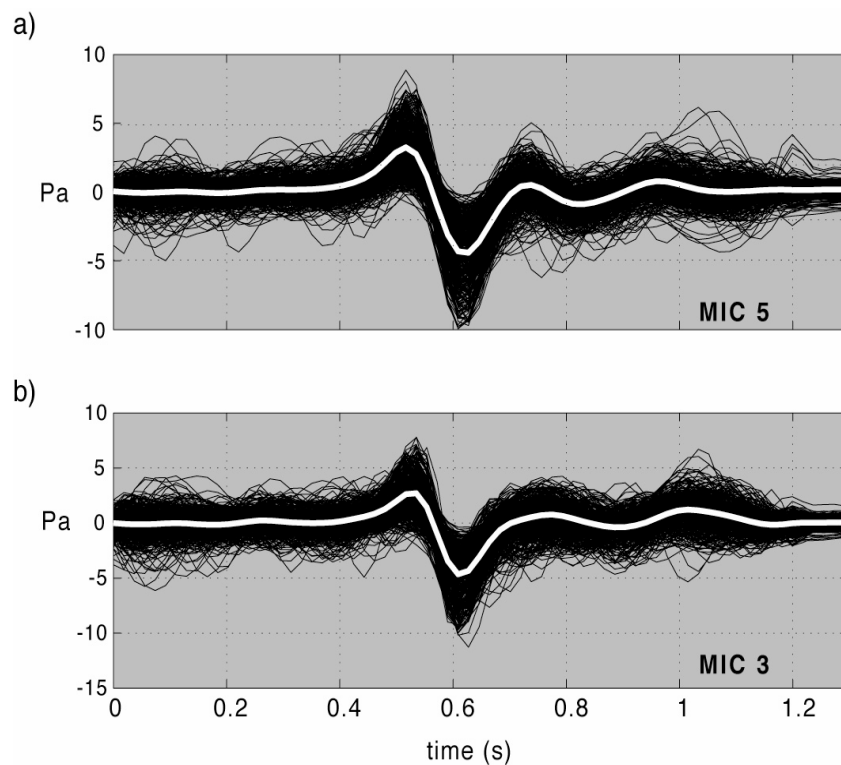


Figure 19. Stacking of ~ 1.200 infrasonic puffing waveforms recorded at a) MIC3 and b) MIC5 elements of the array (Figure 10). The waveforms are extracted using semblance analysis (equation (6)) and selected in a wide range of amplitudes (0.8-9 Pa) during a 3-hour interval of intense activity (February, 13 2004, 21:00-24:00). Deconvolution of the instrumental response was applied. A strong stability of the waveform and duration is evidenced.

For a simple mechanism consisting of a sudden gas bubble expansion at the free magma surface, as the one observed during the lava lake degassing at Mount Erebus (Antarctica, Johnson et al., 2004), the generated infrasound recorded at distance was inferred to be proportional to the mass flux from the source, and the amount of mass being to be recovered proportional to the pressurized gas involved in the bubble burst.

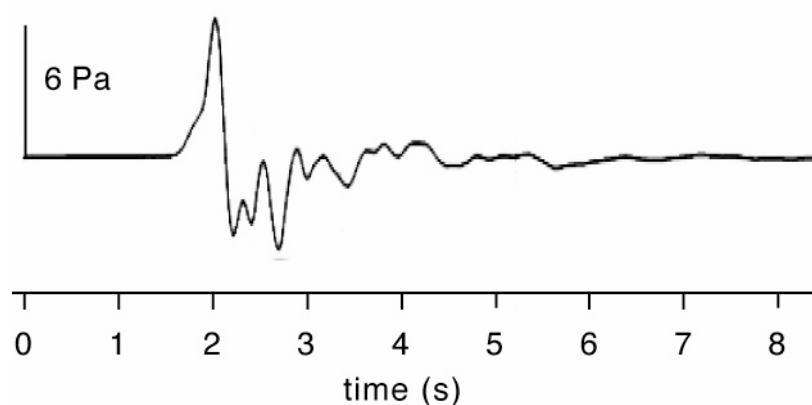


Figure 20. Infrasound signal from the Mount Erebus (Antarctica) lava lake explosion recorded at ~ 1 km of distance from source (from Johnson et al., 2004).

For more complex, long lasting sources of infrasound related to sustained gas discharge from vent, the assumption of a simple gas expansion for the source dynamics is not suitable, and conversion to mass flux is more difficult. In other words, laminar, steady-state gas flow out of a vent should theoretically not generate infrasound. Moreover, the source position within the magmatic column plays an important role in that estimate. An acoustic pressure wave generated inside a shallow basaltic magma conduit by a sudden gas expansion is strongly attenuated by the low elastic module of a magma-gas mixture (Marchetti et al., 2004). As a consequence the amplitude recorded at distance and the estimation of mass will be underestimated. For these cases, hence, the pressure wave recorded at distance is not suitable for estimating gas flux and mass outflow. Although the debate remains as to whether some volcanic infrasound can be generated within the magma column or at the magma/air free surface, the correspondence between the intermittence of the infrasonic pulses (~ 1.8 seconds delay) and that of the gas burst, a 1-2 second delay as evidenced by visual observation and video analysis (Harris and Ripepe, 2007), indicates

that the rapid gas expansion at, or near, the free surface is the more reasonable candidate for the infrasound source. In this case then the infrasonic records should be suitable to recover the mass flux at the origin of the pressure perturbation. Moreover, as the main phase in puffing dynamic is the gas phase with poor magma fragment content, the excess pressure should be entirely proportional to the rate of gas expansion and the amount of gas outflow during a single puff event could be estimated.

Regarding the propagation effects, scattering, reflection, and topography can attenuate the infrasound recorded at distance from the source. In the classical acoustics, the amplitude decay through the atmosphere depends exponentially on the square of the frequency (Reed, 1972). At the wavelength generated by puffing source ($\lambda = c/f$), ~ 100 m for 3 Hz signal and 340 m/s, the effect of scattering and reflection on atmosphere, due for example to ash cloud, is negligible. At short distance, large barometric changes are not expected. However, the presence of a barrier with dimension comparable with the infrasonic wavelength, acting as acoustic shadow, can attenuate the signal. To minimize the attenuation effects, the signal recorded at station #5 (Figure 19) located on line of sight to the active vents has been used in this quantitative analysis (Figure 10).

The simple waveform of puffing recorded at Stromboli allows, hence, simplifying the source model. The infinitesimal pressure perturbation with respect to the ambient atmospheric pressure ($\sim 10^5$ bar) allows to assuming the compressional waves propagating in the elastic domain. As the signals are of ~ 3 Hz of frequency (Figure 19), the generated wavefield has a wavelength (~ 100 m) larger than the source dimension, usually inferred to be of 4-10 m in diameter as the vents. The small source dimension allows to simplify the mechanism of puffing generation as a point source elastically propagating in half space according to the spherical wave equations (1) and (3). According to the linear theory of sound (Lighthill, 1978; Dowling, 1998), for a simple acoustic source, the effective pressure perturbation ΔP should be proportional to the rate of change of mass flux from the source.

For a spherical source with initial radius R_0 (Figure 21) and volume V_0 ($V_0 = \frac{2}{3}\pi R_0^3$) expanding to radius R_1 and volume V_1 ($V_1 = \frac{2}{3}\pi R_1^3$), the mass flux q is

$$q = \frac{dM}{dt} = \Delta V \cdot \rho = \frac{2}{3} \pi (R_1^3 - R_0^3) \quad (8)$$

where ρ is the density of the expanding source.

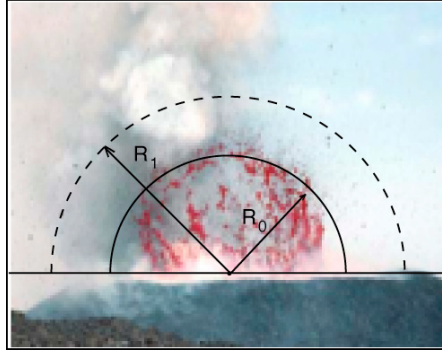


Figure 21. Schematic geometries of a gas expansion with spherical shape. This model of source remember the bubble bursting explosions at lava lake at M. Etna (2001).

The excess pressure due to an acoustic source radiating into a half-space is then (Lighthill, 1978):

$$\Delta P = \left(\frac{1}{2\pi r} \right) \cdot \left[\frac{dq(t - r/c)}{dt} \right] \quad (9)$$

where

$$q = \frac{dM}{dt} \quad (10)$$

Infrasonic records may thus be useful to estimate mass flux for simple sources. From a recorded acoustic pressure signal, a first-order mass flux (kg/s) estimate can be obtained using (Firstov and Kravchenko, 1996):

$$q(\tau) = 2\pi r \int_0^\tau \Delta P \left(t - \frac{r}{c} \right) \cdot dt \quad (11)$$

where τ is the duration of the source function, valid for a monopole source only. In theory, the mass outflow M (kg) is then the time integral of the mass flux rate,

$$M(t) = \int_0^{\tau} 2\pi r \left[\int_0^{\tau} \Delta P \left(t - \frac{r}{c} \right) \cdot dt \right] \cdot d\tau \quad (12)$$

Figure 22 shows a theoretical acoustic pressure recorded at 1.000 m distance from the source (Figure 22a), the time history of estimated mass flux (Figure 22b) and the cumulative mass outflow (Figure 22c) from the source. Assuming a 1 Pa signal (Figure 22a), the expected maximum mass flux is ~ 430 kg/s (Figure 22b) while the total mass output after ~ 0.4 seconds is equal to ~ 110 kg (Figure 22c, white circle).

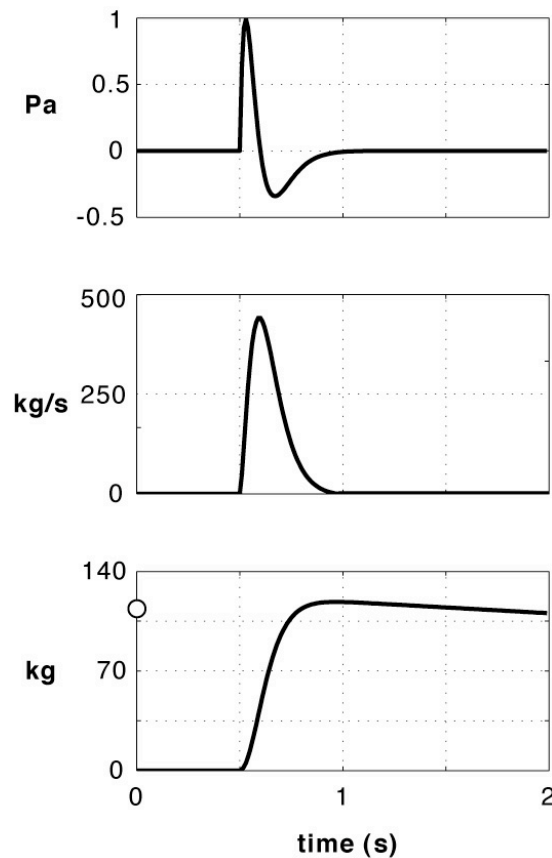


Figure 22. a) Simple synthetic infrasonic, 1 Pa amplitude, signal at ~ 1 km distance, b) the corresponding mass flux and c) the cumulative mass outflow for a point source expanding in half-space. According to equation (12) the total mass outflow is of ~ 110 kg.

Assuming the puffing signal recorded at distance from the source as representative of the time history of the source, the equations (11) and (12) could be applied to estimate the mass flux and the amount of mass involved in each puff, respectively. An example of mass flux and mass outflow estimated for a single puffing signal recorded at ~ 500 m from the active vents is shown on Figure 23.

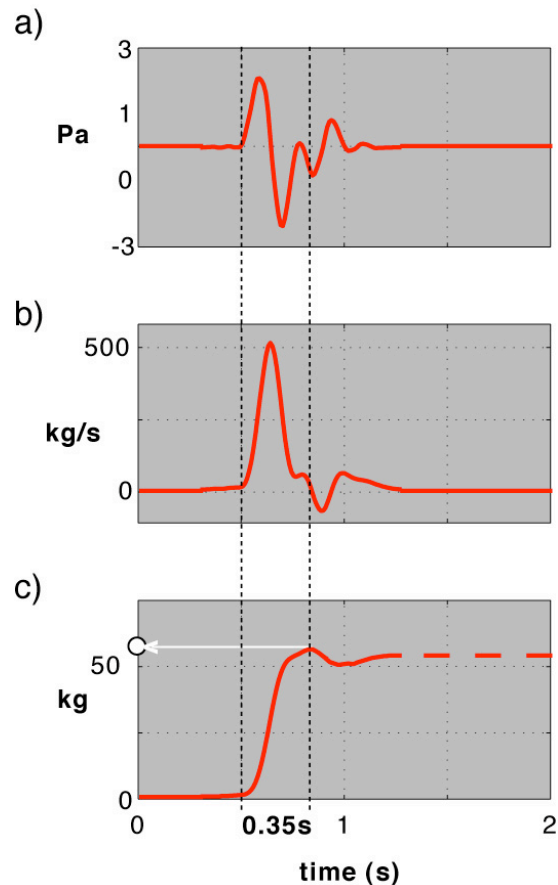


Figure 23. a) Small (2 Pa) infrasonic puffing signal at ~ 500 m from the active vent at Stromboli, b) the corresponding mass flux time history according to equation (11), and c) the cumulative mass flux according to equation (12). The white point indicates the estimated maximum mass (~ 55 kg) emitted.

For a given 2 Pa infrasonic signal (Figure 23a) the time history of mass flux (Figure 23b) revealed a positive onset reaching a maximum value of ~ 500 kg/s. As the main variation of flux lasts ~ 0.35 s and negative mass flux values are physically not possible, only the initial phase (~ 0.35 s) of the puffing signal has been considered (Figure 23a, white patch). The resulted total gas mass outflow is hence represented by the maximum value of the first positive onset of the cumulative mass flow (Figure 23c, white point), equal to ~ 55 kg. In

general, if a steady state mass flow exists after the initial phase of the mass flux, most probably it cannot be recovered by infrasonic data, resulting in an underestimation of the total mass output. In the case of the simple, impulsive and short lasting (~ 0.5 s) pressure signal of puffing, this contribution to the total amount of mass emitted should be minimum.

Therefore, in order to estimate the total gas mass output during the variable active degassing at Stromboli from infrasound, ~ 1.200 waveforms of puffing recorded at station #5 of the array (Figure 19, above) have been divided in several classes of amplitude in the range 1-8 Pa. For each class, the stacked waveform was calculated and a series of representative, low noise, infrasonic waveforms for a wide range of amplitudes (Figure 24a).

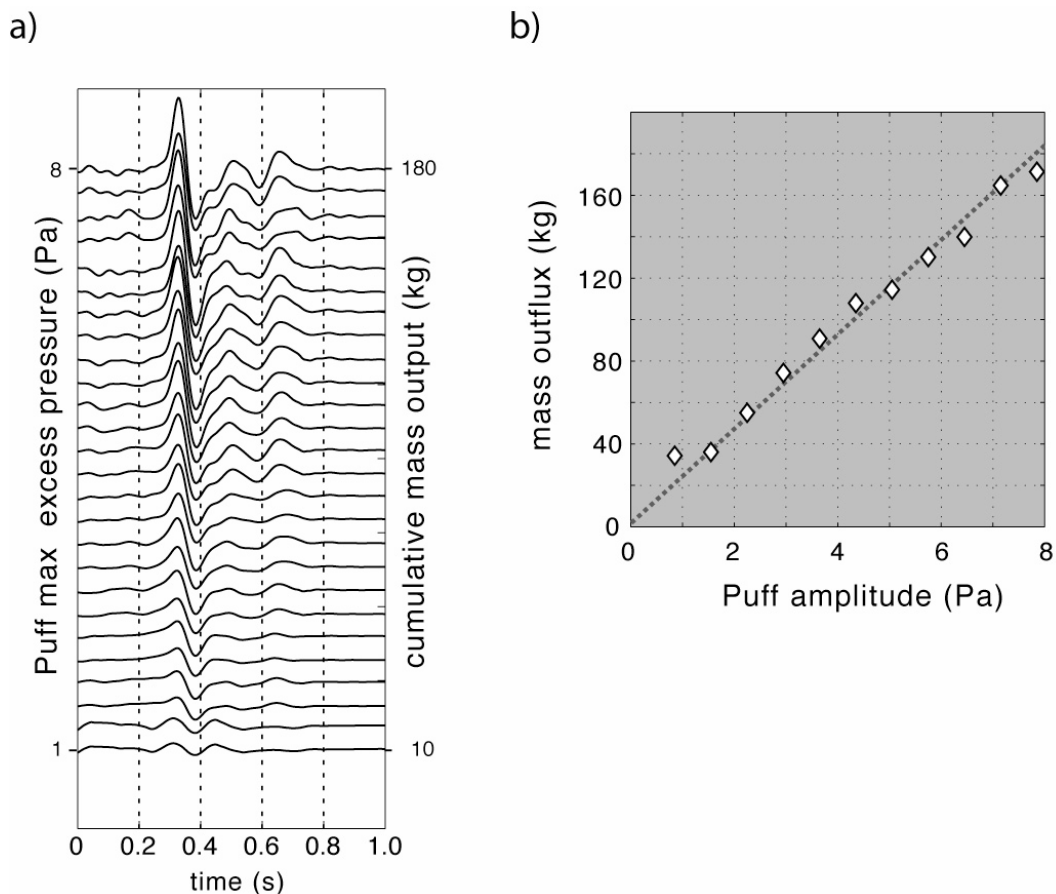


Figure 24. a) Infrasonic puffing stacked waveforms within 1-8 Pa range of amplitude recorded at ~ 500 m from the active vents. Each waveform results from the stacking of ~ 40 signals in each class of amplitude. Within this amplitude range the puffing waveforms show a stable signature and duration (~ 0.5 s). b) Puffing amplitude versus total mass outflow according to equations (11-12).

The total mass output has been then estimated according to the equation (12). As for each stacked waveform the signal duration (~ 0.5 s) and frequency content (~ 3 Hz) are constant (Figure 19 and Figure 24a), a direct relation between the amplitude of the signal and the estimated mass outflow results from the computation (Figure 24b). Within the range of amplitude investigated ($1-8 \pm 0.25$ Pa) the gas mass ranges between 10 and 180 kg. Assuming a mean delay between intermittent puffing signal equal to 1.8 seconds (Figure 15), $\sim 4.8 \cdot 10^3$ events per day contribute to produce the total gas outflow. For such intermittent signals with 2 Pa daily average amplitude, the total gas discharged on atmosphere is ~ 2.000 ton/day. This amount of gas is of the same order of magnitude as gas pollution emitted by the chimney of an important industrial area (~ 1.200 tons) during one year of activity.

As the linear relation between the amplitude of puff event (Pa) and the amount of gas emitted (kg), the characterization of the averaged amplitude of puffing at Stromboli has been evaluated in order to establish the range of gas flow generated by active degassing. For this purpose the infrasonic amplitudes processed in real time at Stromboli since 2003 (Ripepe et al., 2007) have been used. In this case the signals are extracted using the same semblance method (equation (6)) but with 6-second windows with 4 seconds of shift, which strongly reduce the run time process for real time purpose. Within this window of analysis more than one puffing event (~ 1.8 seconds of time delay) will be involved. The resulting amplitude has been calculated as the maximum inside the window. Besides this faster method generates an overestimation of the amplitude, the average daily amplitude is only partially ($\sim 2\%$) affected by this effect. The distribution of the mean daily amplitude of puffing during the 2003-2006 period (Figure 25), shows a mean value of $\sim 2.2 \pm 1.2$ Pa, which can be assumed as the typical amplitude during mild strombolian degassing activity. Frequently wide variations between 1 and 5 Pa are observed during that interval, while only sporadic phases with strong puffing activity with daily amplitude up to ~ 8 Pa are encountered. Within the typical 1-5 Pa range of amplitude, the gas outflow value produced by this type of degassing has been calculated assuming an intermittence range between 3.5 and 1.5 seconds (Figure 17b). For this range of regimes, the active degassing outflow ranges from a minimum of 600 tons/day up to a maximum of 4500 ton/day (Figure 26). For a composition of the Stromboli plume of 80% H₂O, 10% CO₂, 6 % SO₂ and 4% HCl

(Allard et al., 1994), the estimated SO₂ flux is in the range 35 – 270 tons/day, with a mean of ~ 100 tons/day.

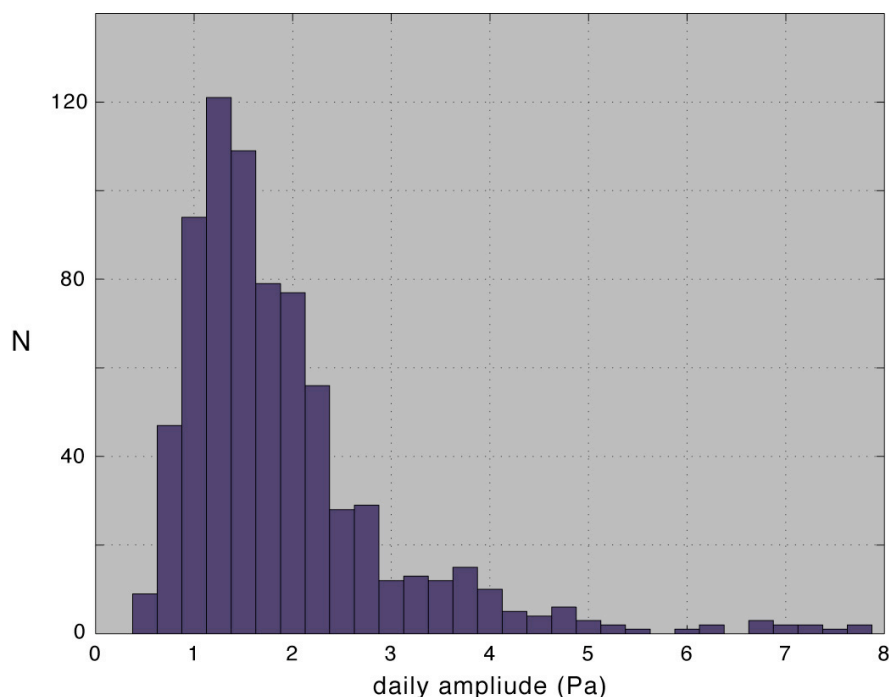


Figure 25. Distribution of daily amplitudes of puffing in the 2003-2006 period. The mean daily amplitude is 2.2 ± 1.2 Pa. Amplitude variations within 1 and 5 Pa range are frequent, while only in few cases the amplitude reach values until 8 Pa.

The estimate of the total contribution of the passive and the active degassing to the SO₂ output at Stromboli, as inferred by spectroscopic in situ sensing methods (Burton et al., 2001; Salerno et al., 2004 and unpublished data), ranges between 50 and not exceeds the 450 tons/day during strombolian activity, while reach up to 1200 tons/day in relation to effusive activity (INGV, unpublished data). By means of spectroscopic remote sensing methods, moreover, Allard et al. (1994) estimated a total SO₂ output at Stromboli of $\sim 10^5$ ton/year, resulting in a daily average of ~ 270 tons/day. The latter estimate should be more representative of the total averaged SO₂ output during mild strombolian activity. Besides a precise comparison between these independent measures of the total gas flux and that estimated in this work should be required combined analysis, taking into account the estimate of Allard et al. (1994) and the average estimate of active degassing carried out in this work (~ 100 tons/day), the mean contribution to the total gas output is $\sim 38\%$ of the total SO₂ output, indicating that the active degassing plays a significant role in the total gas

outflow of Stromboli. Besides the assumption carried out in this work for the estimate of gas flow starting from infrasonic data, an analogous order of magnitude of gas flux has been achieved by means of thermal analysis (Harris and Ripepe, 2007).

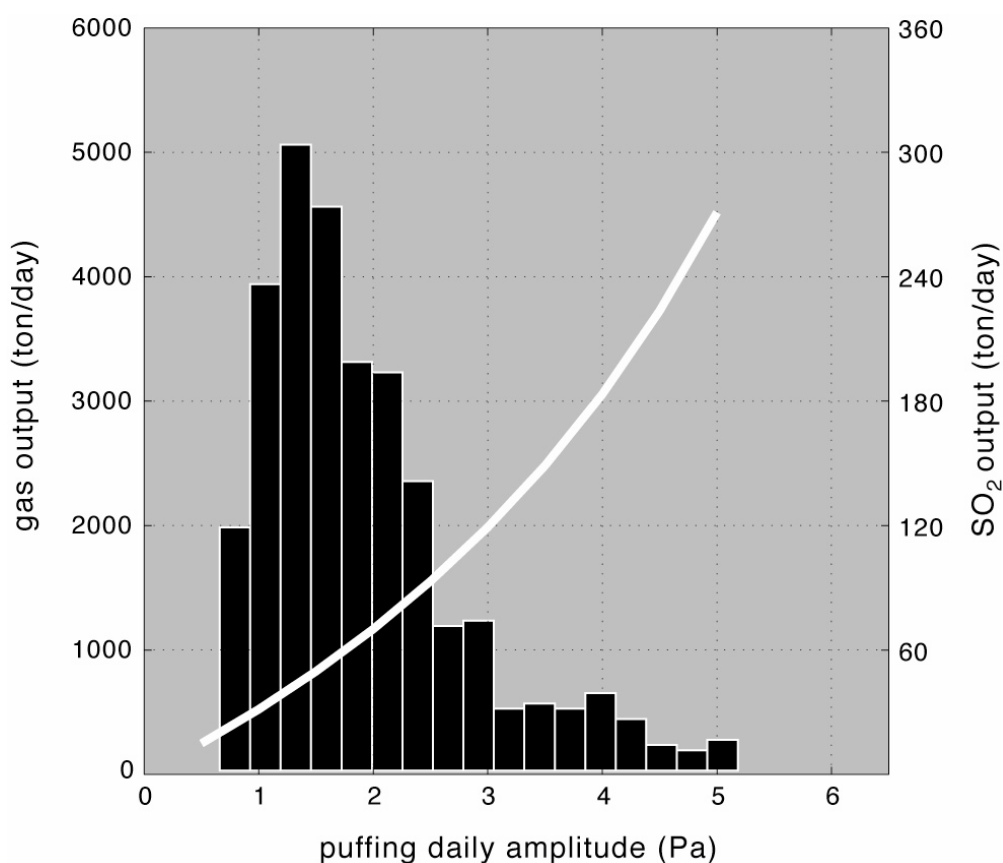


Figure 26. Estimate of the total gas output (ton/day) due to the puffing activity as a function of the average daily amplitude (Pa) for mild to high strombolian degassing (Figure 25). For the computation of the total daily gas flow a 3.5 to 1.5 mean intermittence (s) of puffing in the 1-5 Pa range has been considered. The total gas output has been converted in SO₂ gas output considering a 6% concentration (Allard et al., 1994). For the range of daily amplitudes typically observed at Stromboli (bar plot), the gas output varies between 35 up to 270 tons/day. The mean amplitude of puffing is 2.2 Pa (Figure 25) corresponding to an average of ~100 tons/day of SO₂ flux. The active degassing during mild degassing activity accounts for the 38% of the total gas outflow at Stromboli (10⁵ tons/year or 270 tons/day, Allard et al., 1994).

The behaviour of the source location

Following the numerical procedure previously described, back-azimuthgram (Figure 13) reveals the presence of infrasonic activity around the array and allows to easily track changes in the activity at several vents. On volcanoes such as Stromboli where several vents can be active at the same time, monitoring the back-azimuth direction of infrasound is a powerful procedure to track and visualize changes of activity in the crater area (Ripepe et al., 2007).

In order to characterize the source of infrasonic puffing the analysis of infrasonic back-azimuth was carried out on the dataset since 2004. Within this period three main different behaviours of the puffing source position have been observed at short (hourly to daily) time scale (Figure 27).

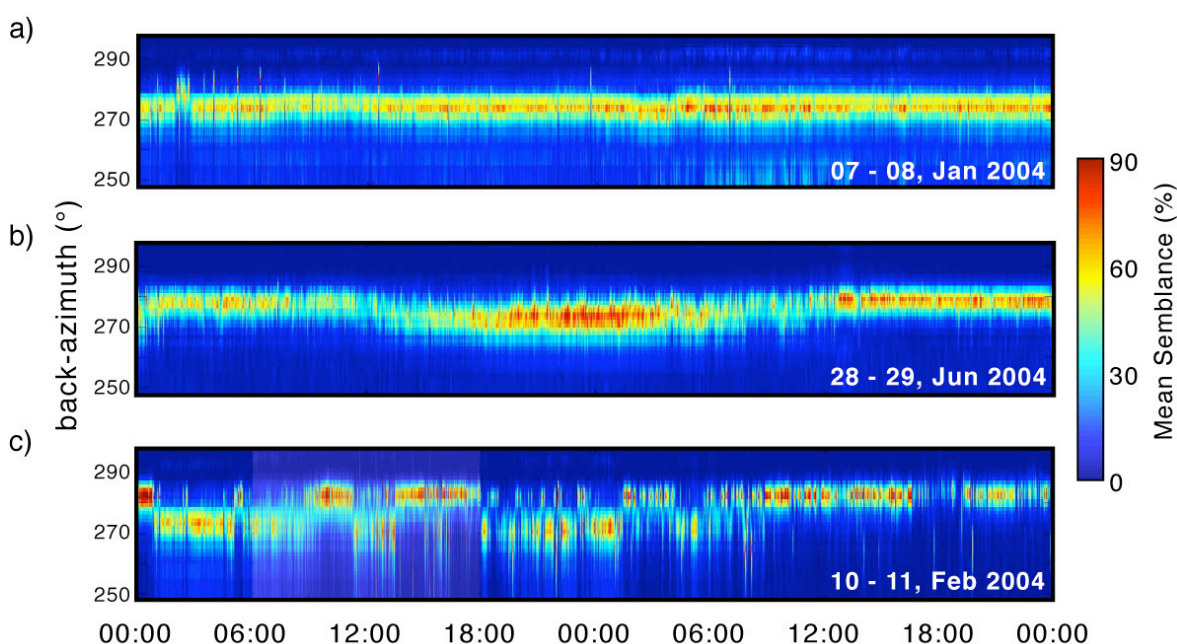


Figure 27. Three samples of infrasonic back-azimuthgrams during 48 hours of typical Strombolian activity at Stromboli (a-b-c). Colorbar represents the mean semblance (equation (6)) across the array calculated on 5-second window. The high (> 60%) semblance values during the 48 hours are indicative of the sustained active degassing. The position of active degassing within the crater terrace (Figure 10) shows three main different behaviours: stable at single vents (07-08 January, 2004) or shifting from vent to vent with smooth (28-29, June 2004) or abrupt (10-11 February, 2004) transition.

Infrasound location indicates that this process is active only in one vent at once. Location of the puffing is stable in a single vent over hours-to-days periods (Figure 27a), or it can

shift from vent to vent with smooth (Figure 27b) or abrupt transitions (Figure 27c). However, the smooth transition is related to a shift between very close vents corresponding to little backazimuth angle ($\sim 5^\circ$) compared to the one related to abrupt shift ($\sim 10^\circ$), resulting in a smooth effect rather than a real gradual transition. The stability in the position of the puffing within the crater terrace suggests that the over-pressurized gas bubble flow is following only one preferential segment of the feeding conduits at once. The stable location of the bursting bubbles, however, may change from time to time and without any apparent evidence or trigger mechanisms, leading to a sharp change in the rising path of gas bubbles.

This gas bubble behaviour seems to be consistent with experimental and numerical studies on the partitioning of particles and drops at pipe bifurcations (Figure 28).

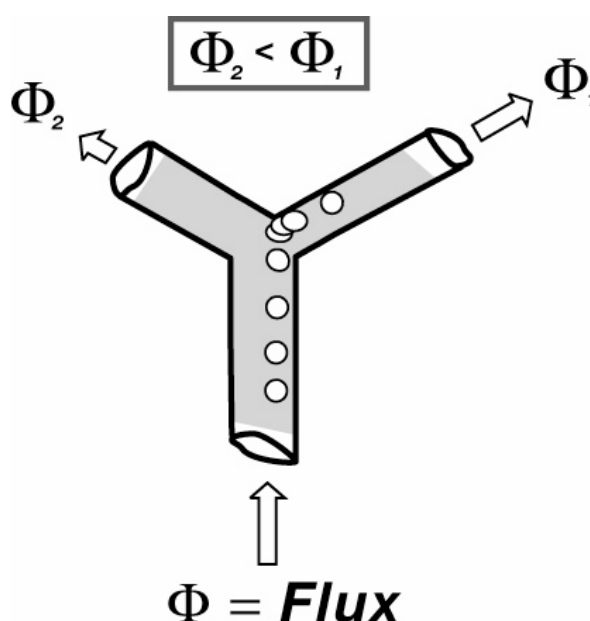


Figure 28. The motion of a train of rising bubbles in a dense fluid approaching a bifurcation has been investigated numerically and experimentally for studying hydrodynamic processes like the gas transport on cardiovascular circulation. The motion of suspended phase depends on many parameters but in general a train of gas bubble tends to follow the high-flow rate channels. The distribution of the location of the active degassing observed at the multi-vents system of Stromboli seems to be consistent with experimental and numerical studies on the flow of particles and drops at pipe bifurcations.

In complex pipe geometry, gas flux is related to the particle volume fraction and to the form of the node (Ditchfield and Olbricht, 1996; Manga, 1996, Stark and Manga, 2000), whereas suspended particles and bubbles tend to favour the high-flow branch of

bifurcations. In the experiments it is clear how, in the presence of multiple bifurcations, gas bubbles and particles are rising in the pipes following trajectories coinciding with the branch that has the highest gas flux. Over-pressurized gas bursting would thus not only reflect the higher gas flux regimes in the conduit but also indicate where the gas flux is more localized within the volcanic system. Accordingly, infrasonic monitoring on multi-vents active volcanic systems not only helps to detect the explosive intensity but also to track the position of the gas flux regime.

Over a longer time period, the location analysis allows to identify a further character of the puffing activity. Between March 2003 and December 2005, the real-time array analysis led to locate ~ 23 millions of infrasonic transients, considering both explosions and small amplitude infrasonic pulses. To evaluate the average behaviour of the source position of active degassing, the average hourly back-azimuth, reflecting the position of sustained (active degassing) rather than the transients (explosions) process, and the source location density within the crater terrace for the 2003, 2004, 2005, 2006 interval have been calculated (Figure 29). The source location density (Figure 29) points to the peak of infrasonic activity located in the NE crater for the 2003 period (~ 5.4 millions events, Figure 29a), while it is consistent with that of the Central crater for 2004 (~ 7.0 millions events, Figure 29b), 2005 (~ 2.5 millions events, Figure 29c) and 2006 (~ 8 millions events, Figure 29d). The Central vent hence, represents the most common source of active degassing at Stromboli.

The behaviour of the position of the active degassing within the crater terrace suggests that the over-pressurized gas bubbles flow is following only one preferential segment of the feeding conduits at once, typically localized in the Central portion of the crater terrace.

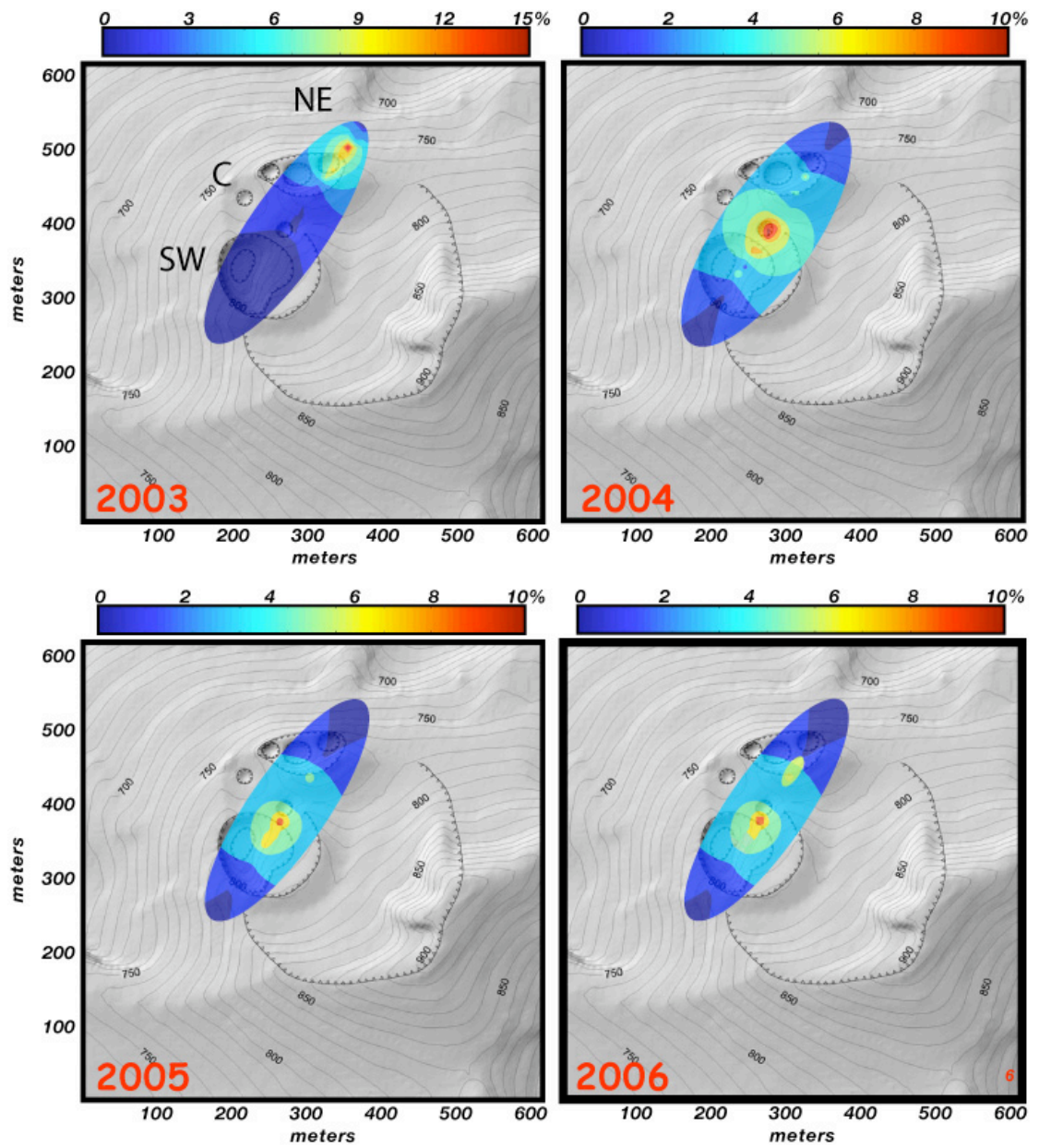


Figure 29. Density of infrasound locations over the crater terrace during the 2003-2006 period, which evidences the preferential location of the puffing source at the Central vent.

4. The dynamic model of active degassing

The analysis of infrasonic puffing activity at Stromboli volcano as evidenced in this work consists of the following main points:

- (1) The source of infrasonic puffing is compatible with a sudden expansion of pressurized gas at the magma/air interface, its amplitude being proportional to the amount of gas released.
- (2) Quantitative estimation of the average gas mass flow indicates that this stationary process plays a significant role in the steady-state degassing budget of the system
- (3) The intermittent regime seems to be driven by the rate of gas flux from depth
- (4) The behaviour of active degassing location within the multi-vents system is compatible with experimental and numerical studies on the partitioning of particles and drops flows at pipe bifurcations

The active degassing at Stromboli hence, can be considered as representative of the pressure perturbation regime inside the shallow conduits system, and any amplitude variations reflect changing in gas flux regime inside the shallow feeding system. On the basis of these results a attempt to model the active degassing at Stromboli has been carried out in this work. A model where the gas flux regime drives the active degassing, in particular the accumulation model proposed by Jaupart & Vergnolle (1988, 1989) on the basis of laboratory experiments, seems to be consistent with the behaviour of this degassing process.

Gas accumulation model

In the laboratory experiment of Jaupart and Vergnolle (1988, 1989) gas bubbles are generated at the bottom of a tank filled with viscous liquid and topped by a small conduit (Figure 30a). Gas bubbles accumulate at the roof of the tank in a foam layer with increasing thickness H_f . At a critical thickness the bubbles are forced to coalesce and then the foam will collapse generating a gas pocket with a size depending on the liquid viscosity μ and surface tension σ . For a given gas flux, two main behaviours of the foam are evidenced at low and high viscosity. At low viscosity a single gas pocket is periodically generated, which will rise in the conduit with an annular flow configuration (Figure 30c), while at higher viscosity only part of the foam will coalesce and rise as slugs with a bubbly flow regime (Figure 30b). In this way the foam will maintain a constant thickness close to a critical value H_c and with an occurrence time t_c of the foam collapse, which will guarantee the steady-state regime in both conditions. The latter behaviour observed in the experiment appears consistent with the regime of puffing inferred for active degassing at Stromboli.

The relevance of this experiment is that the presence of a geometrical constriction can play a significant role in the shallow degassing dynamics far different from the simple passive degassing mechanism. Moreover, their mathematical equations can be used to describe the steady-state regime in term of critical gas flux Q_c (m^3/s) dimension of the pipe r_t (m), intermittence time t_c (s) and dimension of the bubbles R (m) feeding the foam

$$Q_c \cdot t_c = \pi \cdot r_t^2 \cdot \left[\frac{2 \cdot \sigma}{R} \right] \cdot \left[\frac{1}{\rho_l \cdot g} \right] \quad (13)$$

where σ is the surface tension (N/m) and ρ_l is the density of fluid (kg/m^3).

Besides the complexity of the natural volcanic system, the direct relation between time of occurrence and flux regime in equation (13) can be used to explain different explosive regimes observed during either frequent (minutes to hours), low energetic strombolian activity, or in the periodic (days to weeks) fire fountain activity at Kilauea volcano (Jaupart

and Vergniolle, 1988). The longer the periodicity, the longer the burst duration and the released energy.

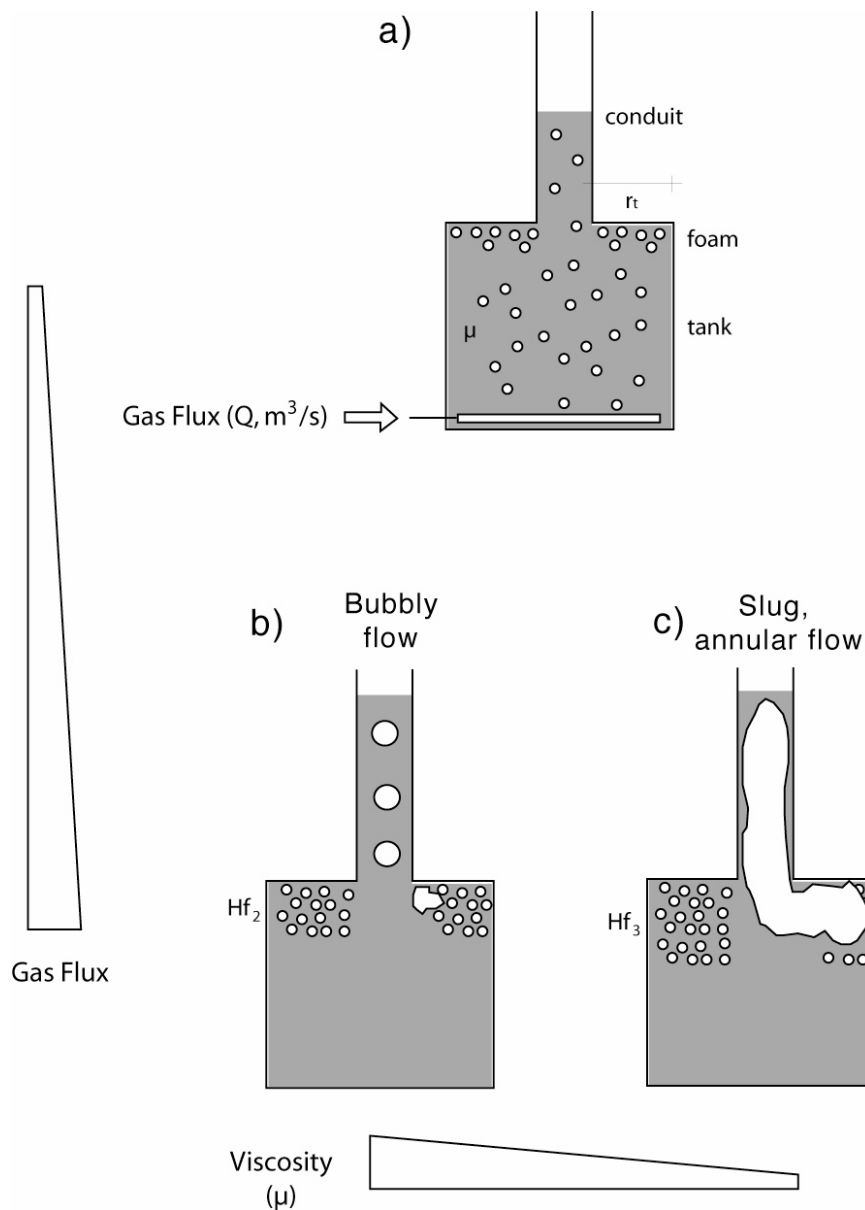


Figure 30. a) Schematic representation of the experimental setup of the foam accumulation model after Jaupart and Vergniolle (1989). A cylindrical tank filled with viscous fluid and topped by small conduit is fed from below by gas bubbles that can accumulate generating a foam layer. Based on the viscosity of the fluid three different regimes, simulate the degassing process in basaltic eruption (Jaupart and Vergniolle, 1988; Jaupart and Vergniolle, 1989). a) Geometries of the system and dynamics of liquid (grey) and gas (white circles) phase. At low gas flux no foam accumulation is generated, producing a bubbly flow regime (a). At a critical gas flux a foam layer H_f is developed. Two different behaviours of the foam layer are observed for high (b) and low (c) viscosity μ of the fluid, intermittent bubbly flow and slug annular flow, respectively.

Recent seismological (Chouet et al., 2003) and ground deformation (Marchetti et al., 2008) experiments have demonstrated that the geometries of the shallow feeding system at Stromboli cannot be assimilated to a cylindrical tank as in the experiment, but rather to a striking NE-SW dike (Tibaldi, 2001). In this case the hypothetical surface where bubbles can accumulate will be an elongated rectangle of length L_d and width W_d .

Equation (13) can be then rewrite for a dike as,

$$Q_c \cdot t_c = \frac{L_d \cdot W_d \cdot 2\sigma}{\rho_l \cdot g \cdot R} \quad (14)$$

The ratio on the right represents the balance between the momentum due to surface tension ($L_d W_d 2\sigma$) and the internal pressure of the bubble ($\rho_l g R$). In the experiment the gas bubbles accumulate at barrier generating a foam level. If the dimension of the tank is small enough and/or the viscosity of the fluid is high, the drag flow of the accumulated bubbles toward the open conduit is small, resulting in the growth of the foam volume. When the accumulation reaches a critical volume, the deformation of bubbles under the action of the buoyancy force promotes the rapid coalescence generating a large gas pocket that will rise in the conduit. In this model hence, the kinematics of foam collapse is controlled by the balance between the buoyancy force at barrier and the surface tension of bubbles in the foam. In the case of an open conduit volcano such as Stromboli, two main hypotheses have to be done in order to apply equation (14): i) the presence of a structural barrier where gas bubbles can accumulate, and ii) the presence of a buoyancy gas foam at some depth which promotes the generation of large gas pockets rising intermittently.

Structural barrier has been invoked to explain the seismic source (Chouet et al., 2003), suggesting that the shallow system, feeding the vents, can be represented by the upper parts of a NE–SW striking, $\sim 60^\circ$ dip, dike (Figure 31), which follows the sliding plane activated during the Sciara del Fuoco collapse (Tibaldi, 2001). The knee of the shallow feeding system (Figure 31) should represent the zone where the ascending gas-rich magma undergoes a change in the fluid-dynamic behaviour. This zone most probably coincides with the location of the volumetric expansion related to the seismic source of the explosive activity (Chouet et al, 2003), located at 200 to 300 m below summit craters. This depth

coincides with the modelled equilibrium pressure of 0.4 to 4 MPa that accounts for the low (<10) CO₂/SO₂ ratio measured in the plume at Stromboli during the normal degassing activity (Aiuppa et al., 2008; Burton et al., 2007a).

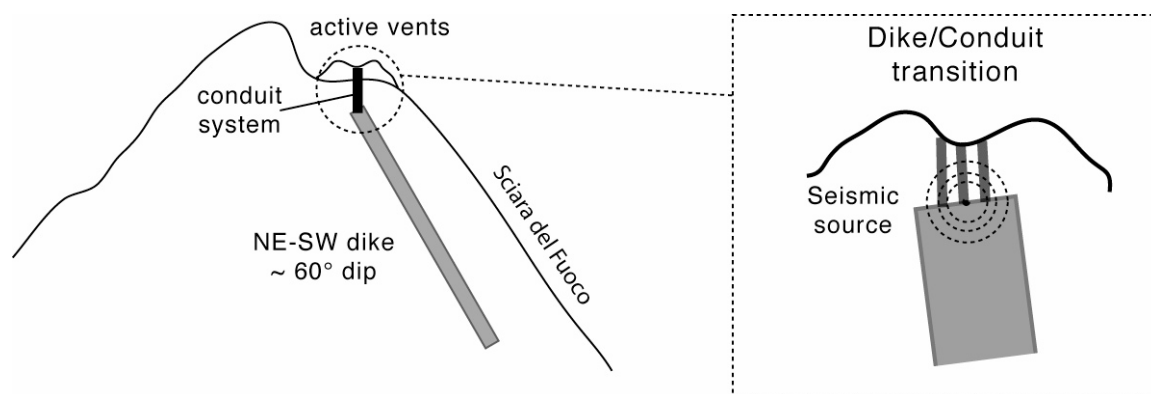


Figure 31. Sketch of the structural setting of the shallow feeding system at Stromboli as inferred by seismic (Chouet et al., 2003) and geo-structural (Tibaldi, 2001) analysis.

The high vesicularity of ~ 40-80 % (Polacci et al., 2007; Lautze and Houghton, 2005) and the foamy texture and the size distribution of bubbles (Polacci et al., 2007) measured on explosive scoria at Stromboli indicate the presence of extensive gas bubble kinematics within the shallow conduit system. Diffusive bubbles growths and coalescence process at the time of fragmentation are invoked to explain the texture observed on the scoria ejecta at Stromboli (Polacci et al., 2007). The generation of gas pocket in the vesiculated basaltic magma such as the one observed at Stromboli however, is limited by the higher viscosity and inertia forces (i.e. Proussevitch et al., 1993) than the one acting in the laboratory experiments of Jaupart and Vergnolle. The interaction dynamics between gas, liquid and solid are complex and an accurate description of it is left for future study. In this work the generation of gas pocket at vesiculated level has been assumed, and the simplified equation (17) has been applied in order to model the active degassing regime.

At Stromboli, gas bursting at every ~2 seconds produces ~1600 ton/day of gas mass output. Assuming that the density of the puff ρ_g is approximately 0.35 kg/m³, equal to that of steam at 625 K (~ 350°C) and atmospheric pressure, the average gas volume output will be of ~55 m³/s. At steady state regime this output flux should equilibrate the input gas from depth. Assuming a magma density ρ_l of 2700 kg/m³ and a surface tension σ on

bubble film of 0.4 N/m (Walker and Mullins, 1981), which represents the standard value for basaltic magma, the unknown variables to solve equation (14) are the three parameters R , L_d and W_d , which represent the requested bubble size and the dimension of the dike, respectively.

A mean bubble size representing the magma vesiculation before the fragmentation process could be inferred from the bubbles size distribution measured in scoria ejecta. By means of classical techniques of optical and scanning electron microscopy of conventional thin section (Cashman and Mangan, 1994) and recent X-ray microtomography imaging (Polacci et al., 2006 and 2007), the reconstruction of the texture and shape of bubble phase in melt erupted at Stromboli evidences a wide range of bubble size, from micrometers to millimetre size (Lautze and Houghton, 2005; Polacci et al., 2006 and 2007). The presence of smaller bubbles in scoria products indicates that the process of nucleation is acting at the fragmentation time, while the presence of larger bubbles reflects the growth process before the shallow magma fragmentation. However, in the explosive products a consistent degassing (loss of bubbles) process should be expected, which could indicate a modification in the vesicle distribution. On Figure 32 are shown two backscattered-electron images of scoria, representing two end-member textures typically observed on products of strombolian activity.

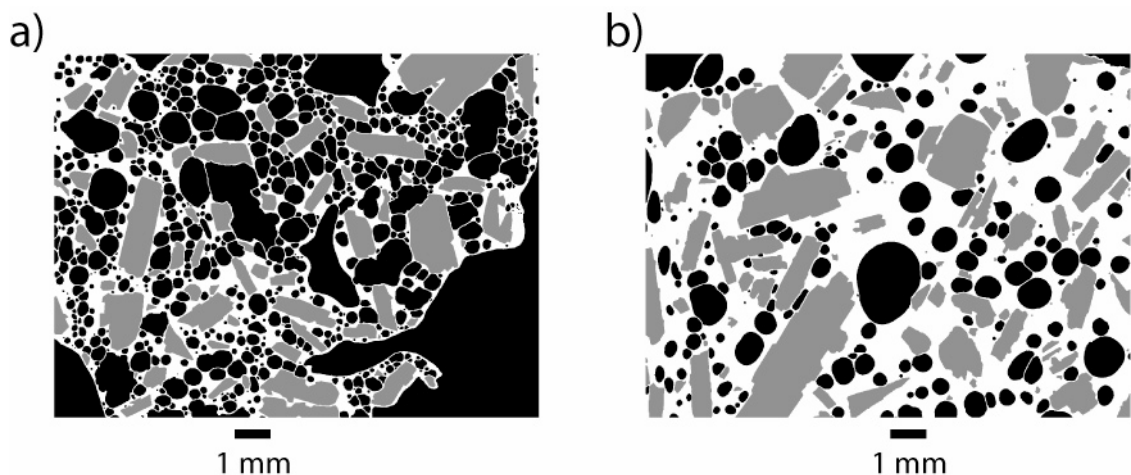


Figure 32. Scanning electron microscopy images showing the texture of multiphase, glass (white), gas bubbles (black) and crystal (grey), in bombs from Stromboli mild activity (June 2008). End member examples of high (a) and low (b) vesiculated magma at Stromboli at the time of fragmentation.

Low mean size with high volume density (Figure 32a) versus high mean size with low volume density (Figure 32b) reflect two distinct vesicle population. In a dynamical model the two end-members have been interpreted in terms of residence time within the shallow conduits system. In this perspective, the low vesiculated portion of scoria (Figure 32b) represents long-residence shallow melts while the high-vesiculated portion (Figure 32a) should maintain the texture of a deeper melt that does not undergo protracted degassing process. Based on these observations the vesicles population observed in Figure 32a better reflects the full vesiculation process of shallow magma at Stromboli and has been used to give the range of bubble size required by the model (R , equation (14)), that is 0.3-0.5 mm (Lautze and Houghton, 2005).

Assuming this bubble size the range of plausible width and length of the dike can be calculated according to equation (14) (Figure 33).

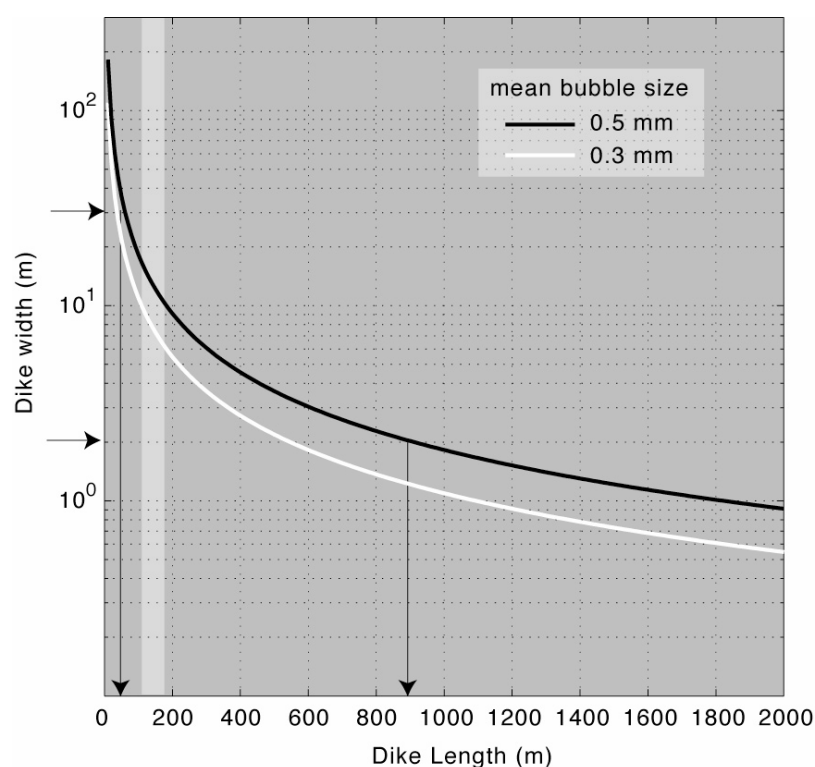


Figure 33. Range of dike dimensions, in terms of length (L_d) and thickness (W_d) for the minimum and maximum value of bubble size R (0.3 and 0.5 mm, respectively) required by the accumulation model to explain the active degassing regime at Stromboli. Assuming $L_d > 2W_d$, the length ranges between 40 and 900 m and thickness between 2 and 30 m. For ~ 10 m W_d as measured on an old outcropping dike (Figure 34), the dike length ranges between 110 and 170 m.

Assuming that $L_d \geq 2W_d$, that is a rectangular dimension of the dike, its resulting maximum width will be ~ 20 m (Figure 33, dotted line). For a minimum plausible width of 2 m, the dike length L_d ranges from 30 to 900 m. The dike outcropping at Stromboli (Figure 34a) shows a width ~ 10 m (Figure 34b).

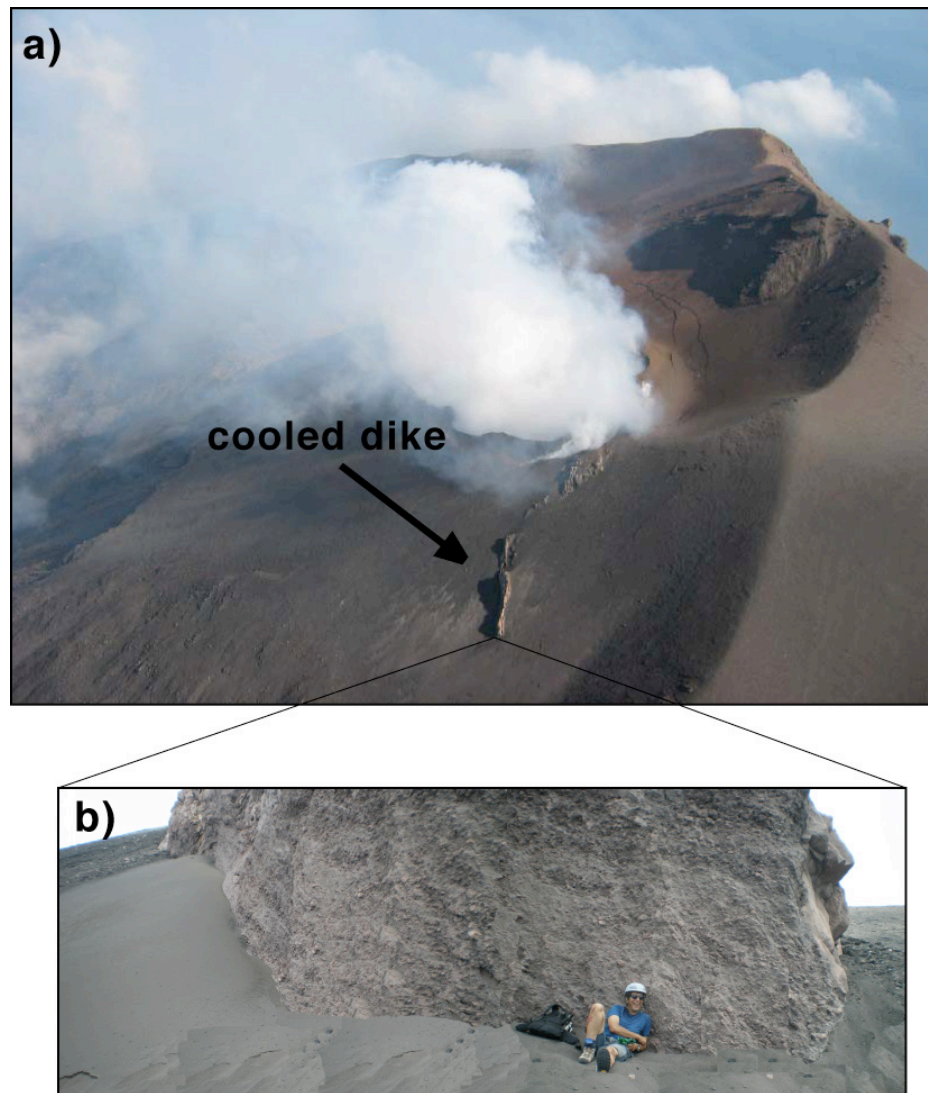


Figure 34. Photos of Stromboli summit crater taken from south (Mar 2007), showing the outcrop of a solidified basalt dike with an E-W strike (a) and ~ 10 m of width (b).

In this case, for the ranges of bubbles size taken into account the length L_d of the dike will be limited to a range of 110-170 m. This dimension represents the higher horizontal extension of the deep dike, which is connected with atmosphere through a system of three main active vents (SW, C, NE, Figure 6 and Figure 10). A coherent variation of the

explosive activity at each vent has been observed at Stromboli (Ripepe et al., 2005), demonstrating that a shallow dike feeds all the active vents. As the extension of the crater area in the NE-SW direction is ~230 m, the projection of the dike will be within the active crater's area.

The proposed model for the shallow feeding dike at Stromboli

Based on geo-structural constrain (i.e. Tibaldi et al., 2001) and geophysical investigation (Chouet et al., 2003; Ripepe et al., 2005; Marchetti et al., 2008) the shallow feeding system at Stromboli is represented by a NE-SW striking dike with $\sim 60^\circ$ of dip toward NW (Figure 31). The uppermost portion of such a dike has been imaged as a system of vertical conduits connecting the magma to the surface. An accumulation of exsolved gas bubbles at the transition between inclined dike and vertical conduit (built-up level) has been hypothesized. Accumulation accounts for the excess of gas mass observed on surface in relation with explosive activity, which is composed of abundant gas then melt (up to 16 in mass, Chouet et al., 1974). Modelled SO_2/CO_2 ratio measured in gas plume during normal degassing (Burton et al., 2007; Aiuppa et al., 2007), limits the depth of the exsolved gas supplying the plume above ~ 4 MPa (<150 m, Burton et al., 2007; Aiuppa et al., 2007). In the proposed model, this depth represents the level of gas accumulation where extensive vesiculation processes should act and drive the generation of gas pocket larger than the original bubble. Under the action of buoyancy force the gas pockets are forced to rise within the shallow conduit and then to burst at the magma-air interface. This is the source assumed for the generation of intermittent (1-2 seconds) pressure perturbation ΔP recorded as infrasonic puffing. This minor overpressurized degassing ($\Delta P \sim 0.1$ bar), called active degassing, is typical of Stromboli activity and account for $\sim 38\%$ of the total gas output measured on plume (Allard et al., 1994). This degassing activity operates alongside with the passive degassing, and reflects the steady-state regime of pressure perturbations within the shallow magma column. In a simplified model where the generation of gas pocket is driven by the buoyancy force at the conduit roof and by the surface tension of bubbles (Jaupart & Vergnolle, 1998), the requested dike dimensions at roof should be ~ 150 m length for a ~ 10 m dike for bubble size in the range 0.3-0.5 mm (Lautze and Houghton, 2005). The active degassing is located at a single vent at once, typically within the Central crater. Its location hence indicates a zone within which the feeding conduit is more fluidized by gas. Any variation in terms of amplitude and source location of active degassing should indicate a change in gas flux regime inside the shallow feeding system. The summary of the model has been schematized on Figure 35.

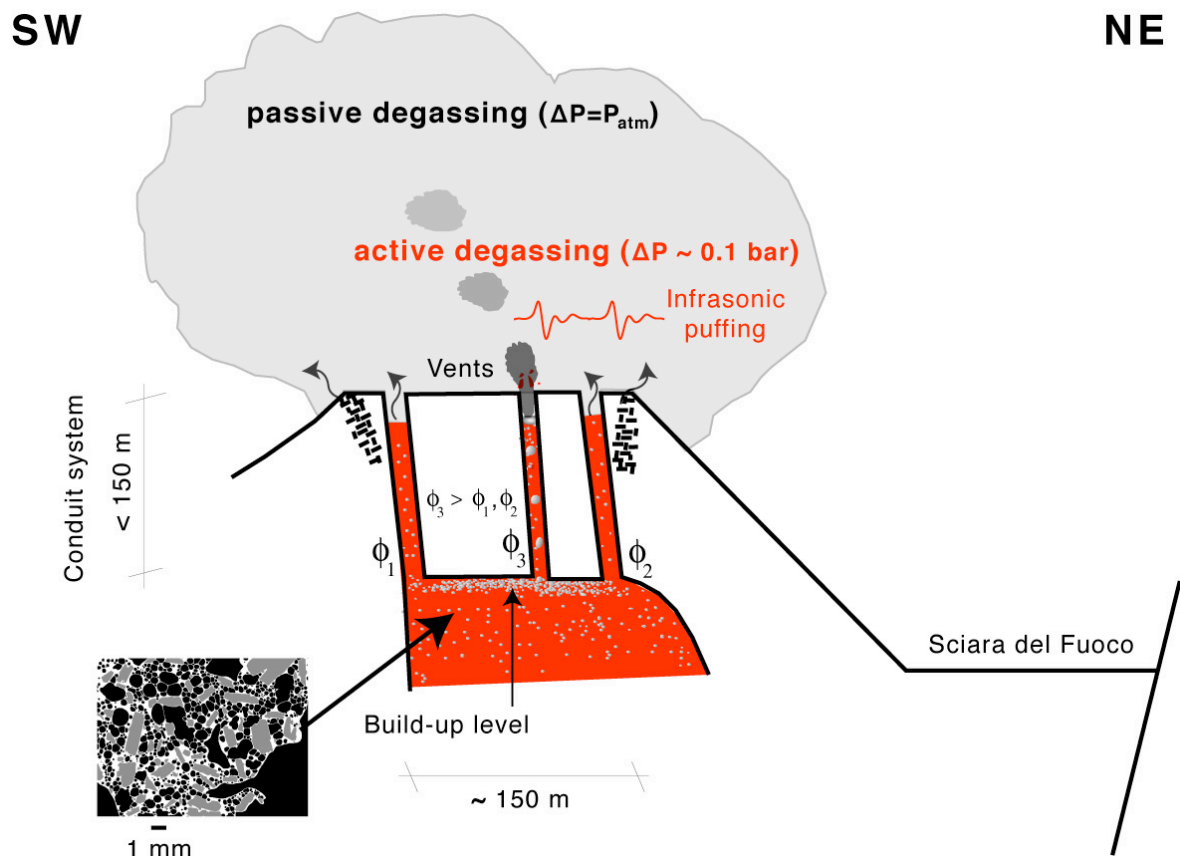


Figure 35. Schematic model of active degassing at Stromboli volcano.

The transition from explosive to effusive in 2006-2007

At many active volcanoes the onset of an eruptive phase is attributed to an increasing of the magma input rate from depth. At Stromboli as in other basaltic volcanoes the transition between the typical explosive and the effusive activity has been attributed to an increase in the magma supply such that which exceeded the typical rate of $0.3 \text{ m}^3/\text{s}$ (Ripepe et al., 2005), and caused the opening of effusive fractures (Buonaccorso et al., 2003).

The active degassing reflects the gas flux regime within the shallow system of conduits and allows to track where the preferential path of the gas flux is located. An increase of the magma input should increase the rate of gas supplying the shallow feeding system, increasing the amount of gas phase and changing its kinematics. The analysis of the behaviour of active degassing during the 2007 explosive to effusive transition (Ripepe et al., 2008) has been included in this work in order to examine the dynamics of the shallow magma column at changing magma input rate.

Since 2003 the Department of Earth Science of the University of Florence has developed an integrated geophysical network to monitor in real-time the variation of the explosive activity at Stromboli volcano (Ripepe et al., 2004). The network (Figure 36) consists of 5 seismo-acoustic stations equipped with broad-band seismometers (CMG-40T, 800 V/m/s and 30 s of eigenperiod) and infrasonic microphones (50 mV/Pa in the 1-20 Hz range); an infrasonic array (FIG); 1 thermal camera FLIR A20 sampling at 1Hz; 1 thermal radiometer OMEGA; 2 tiltmeters Pinnacle 5000T sampling at 1 Hz with a sensitivity of $1 \mu\text{rad}$. All the data are transmitted to and collected, processed and visualized in real-time at the recording center of the National Department of Civil Protection located in the Semaforo San Vincenzo at Stromboli (COA, Figure 36). The benefit of the integrated network is to easily and quickly cross-check all the information together for both the internal (seismicity and deformations) and external (infrasound and thermal) volcanic process related to the ongoing dynamics (Ripepe et al., 2008). During the effusive eruption of February 2007 the information returned in real-time by the different parameters allow an integrated description of the pre-sin- and post-eruptive evolution. In particular, the information returned by the thermal camera has been used in this work in order to integrate the information returned by the infrasonic array during the 2007 eruption.

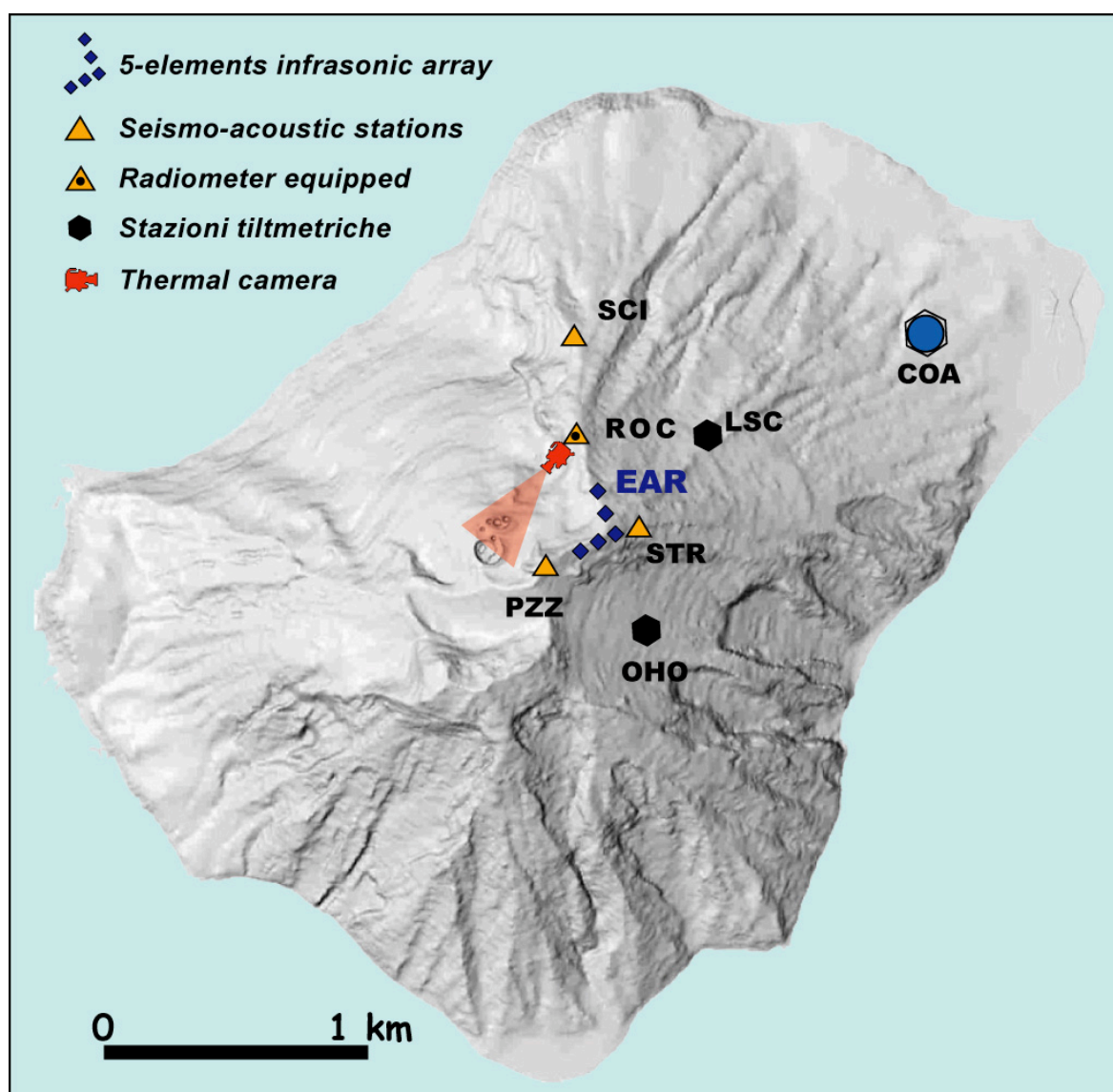


Figure 36. Position of the seismo-acoustic stations (triangles) and radiometer sensors (triangle with black point), 5-elements infrasonic array (diamonds), tiltmeters (hexagons) and thermal camera (camera) of the integrated geophysical network operating during the 2007 eruption. All the data are transmitted, collected and processed in real-time to the recording center (COA) of the Department of Civil Protection located in Semaforo San Vincenzo.

The onset of the effusive eruption has been preceded by an increase of thermal and infrasonic activity (Figure 37). In particular, the analysis of thermal images recorded at station ROC of the monitoring network (Figure 36) allows to calculate in real-time the rate of explosions (DelleDonne et al., 2006). Explosive activity at Stromboli is characterized by 5-17 explosion per hour with a mean of 7 events/hour (DelleDonne et al., 2006). This explosive rate defines the mild strombolian activity at Stromboli, which has been inferred

as the result of a quite efficient conduit process related to continuous supply of magma from depth at a mean rate of $\sim 0.3 \text{ m}^3/\text{s}$ (Gilberti et al., 1992; Allard et al., 1994; Harris and Stevenson, 1997). Starting since January 30, 2007, the rate of explosions has increased almost 2 times (Figure 37b), from an average of 190 events/day (~ 8 events/hour) to an average of 345 events/day (~ 14 events/hour), reaching the maximum rate of 800 explosions per day (~ 33 events/hour) on February 27, 2007, morning. This is the main evidence indicating a large increment of magma supply rate almost 1 month before the onset of the 2007 eruption. This increment has been followed by a synchronous increment of the infrasonic puffing amplitude (Figure 37a), from a 1.5 to 3 Pa weekly average at ~ 500 m of distance from the active vents. The strong active degassing activity recorded one month before the eruption is in agreement with the increased magma input rate, which guarantee a larger gas flux rate in the shallow feeding system. Infrasonic activity monitor by means of array analysis indicates moreover an abrupt change of the position of the degassing activity from the summit vents, coherent with a shift from the typical Central crater to the NE crater (Figure 37c), decidedly indicating a modification of the preferential path of gas outflow in the shallow system of conduits in relation to the increased gas flux rate. The coherent change of the explosive rate and the location and intensity of the active degassing (Figure 37) since 1 month before the eruption is consistent with an important gradual increase of the magma input rate from depth before the eruption.

The precursory, strong, degassing activity reached a maximum intensity in the morning of February 27 and suddenly stopped just before the opening of an effusive fracture at $\sim 13:00$ GMT, indicating that the intensity of the degassing of the shallow magma column (active degassing) and the strombolian activity are strongly coupled. The dynamics observed in the last hours before the 2007 eruption helps us to depict a model of the eruption at Stromboli.

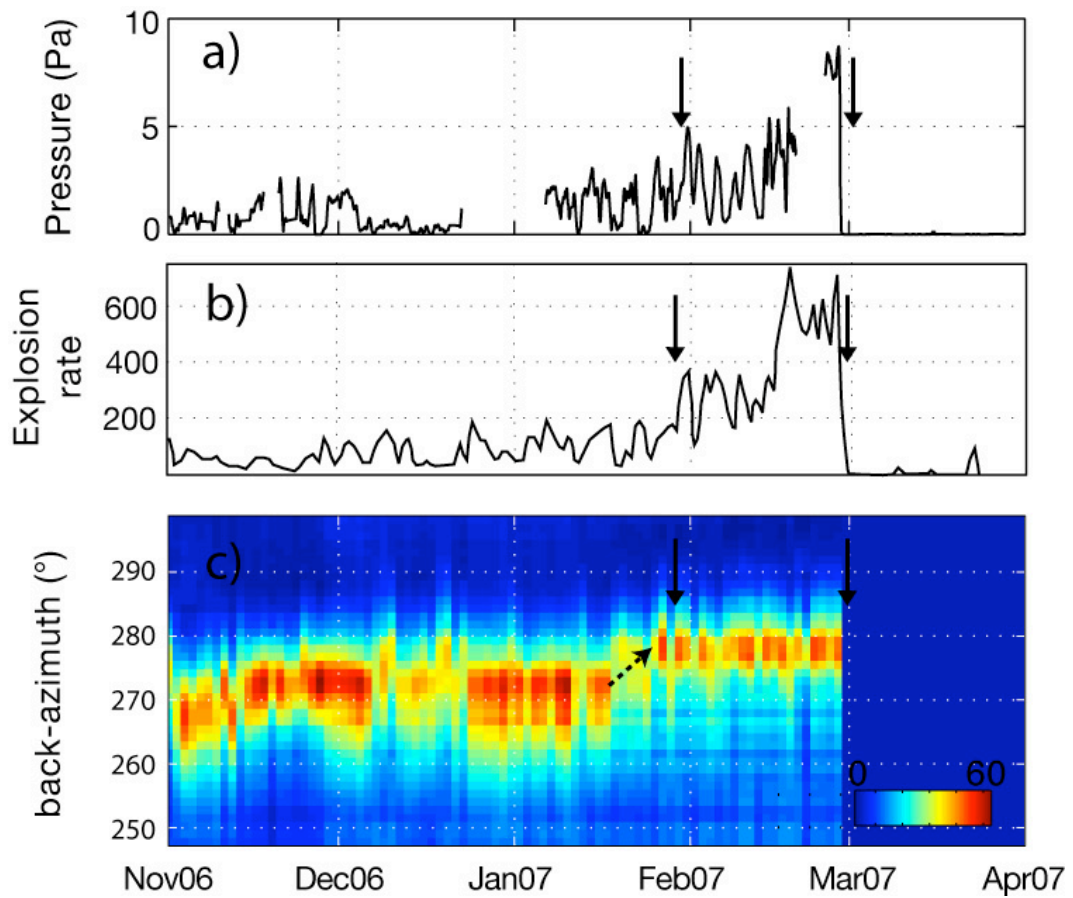


Figure 37. The 5-month-long trends of the infrasonic puffing activity, in terms of a) amplitude and c) source location (back-azimuth), and b) explosive rate across the onset of the February 27 2007, eruption. Pressure amplitude refers to the amplitude of active degassing. The downward arrows indicate, from left to right, the sharp (almost double) increasing of the explosive rate on January 30 and the onset of the effusive activity on February 27, respectively. The dotted arrow indicates the direction of shift of the back-azimuth from SW to NE direction at the end of January 2007.

The propagation of a NE-SW dike and the drainage of magma from shallow conduits

During the last hours before the effusive activity, the intensity of the active degassing (~ 6 Pa of the hourly average, Figure 38a) and the rate of strombolian activity (7-13 explosions/hours, Figure 38b), both localized mainly on the NE crater (Figure 38c), was very high.

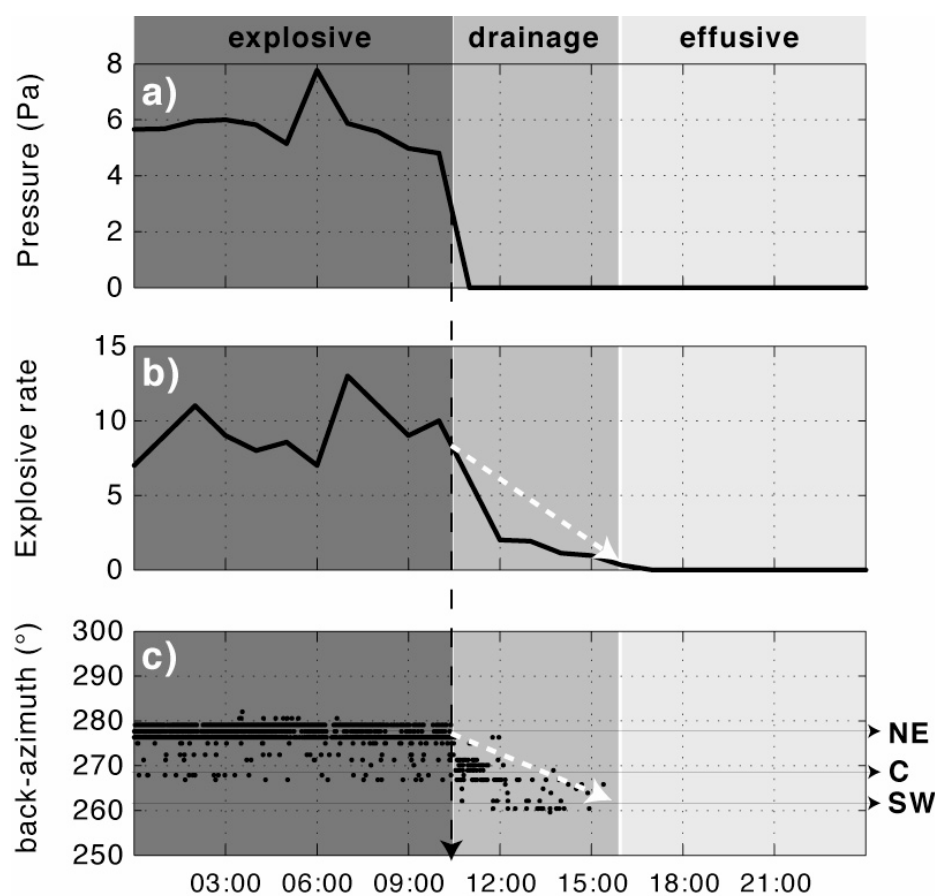


Figure 38. A record 24-hours-long (Feb, 27 2007) of infrasonic puffing activity, in term of amplitude (a) and back-azimuth (c), and explosive rate (b), during the transition between typical, very high, and explosive to effusive activity. The transition from high explosive activity to effusive phase has been characterized by an intermediate 5-hours-long period wherein the lava flow from the opened fissure on Sciara del Fuoco coexisted with weak explosions at summit craters (b) the gradual shift the latter from the NE to the SW vent, suggesting a propagating drainage out of magma from conduits toward NE.

At $\sim 12:30$ GMT (vertical dotted arrow) the sustained active degassing stopped while the strombolian activity gradually decreased in intensity until $\sim 15:30$ GMT (Figure 38b). The first intrusion of magma at the base of the NE crater however, occurred at $\sim 13:02$ GMT

(Figure 39) after the incipient fracturing process at the base of the NE crater started since 12:30 GMT, evidencing that the transition toward stable effusive activity was characterized by an intermediate phase where the weak explosive activity at the summit vents (C and SW) and lava flow from the effusive fissure at the base of the NE crater coexisted.

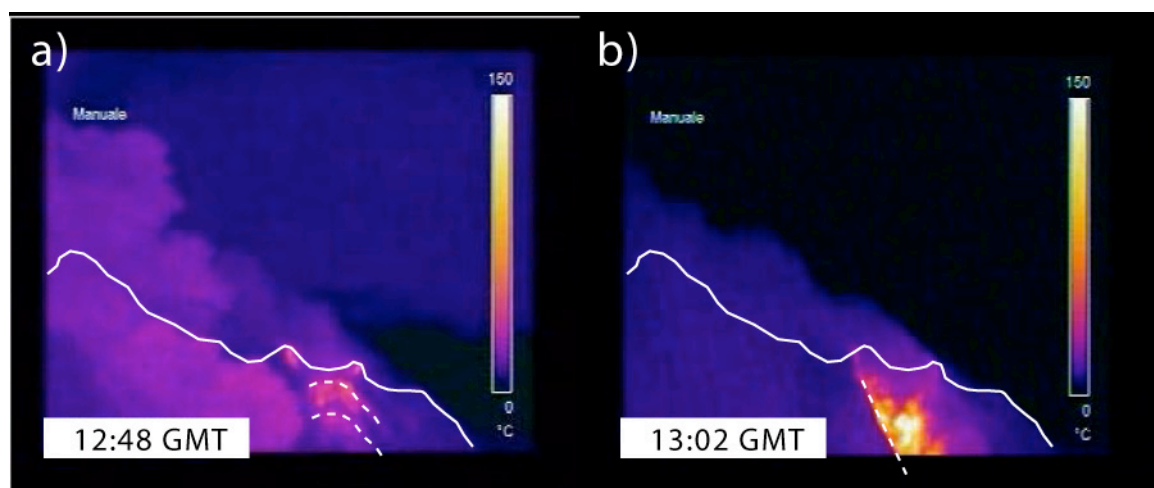


Figure 39. Thermal images from station ROC (Figure 36) on February 27 2007. a) At 12:48 GMT incipient fractures with concave shape were evident at the base of the NE crater. b) At 13:02 GMT thermal anomalies of linear shape suggest the intrusion of magma at the base of the NE crater.

This decrease in intensity of the explosive activity is followed by a gradual shifting of the infrasound back-azimuth toward SW (Figure 38a), indicating a progressive reduction of the explosive activity from the NE to the SW vent.

The time sequence and the shifting of the explosive source within the crater terrace traced by infrasonic array (Figure 38c) suggest that the shallow feeding system was progressively reducing the explosive and degassing intensity while it was moving from the NE towards SW. This kinematics of the explosive activity within the crater terrace is consistent with the image of a shallow feeding dike that is draining magma out of the crater zone by propagating effusive fissures from SW towards NE (Figure 40).

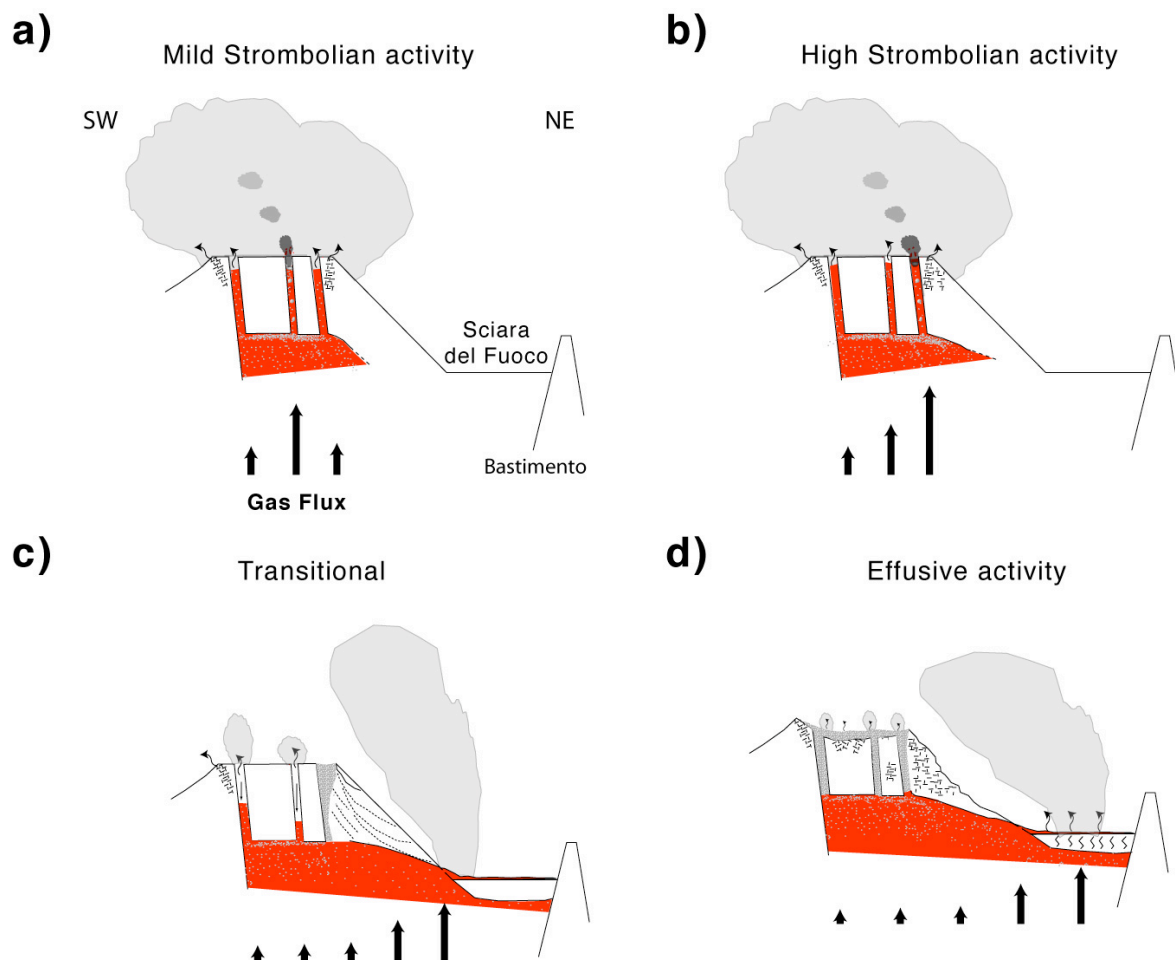


Figure 40. Dynamic model of the 2007 explosive to effusive transition. See text.

5. Conclusion

The present thesis deals with the analysis of infrasound data of persistent degassing activity at Stromboli volcano. Open conduit volcanoes such as Stromboli, are an efficient source of low frequencies (0.1-10 Hz) acoustic wave (infrasound) produced by the release of pressurized gas from active vents during to explosive activity. Compared to seismic, infrasound provides better information on the dynamic of explosive source as its propagation in the homogeneous atmosphere induces less scattering effects. Moreover, the use of small aperture infrasonic array allows precise location of the source and the monitoring of changes in explosive activity at multi-vents system.

Activity at Stromboli is characterized by mild explosions of incandescent gas and bombs, with a variable amount of ash. Between and during strombolian explosions, gas emission persists to feed a steady plume of gas. Gas emission has predominantly an origin in the degassing of magma with emission concentrated in the open vents, as well as fumaroles and fractures on the inner and outer flanks of the crater structure. Besides passive degassing at active volcanoes with persistent activity is believed to be responsible for degassing of large quantity of magma at Stromboli infrasonic and thermal measurement evidenced an intermittent (1-2 s), low energy (1-10 Pa at ~ 500 m of distance from source) signals (called puffing) linked to the bursting of small hot gas pockets. This degassing mechanism, called *active degassing*, operates in over pressurized condition alongside passive degassing. For the over pressurized condition, the analysis by means of infrasonic array presented in this work, allowed a precise characterization of this shallow degassing mechanism in term of regime, source location and produced gas flux.

The intermittent pressure pulses related to active degassing are quite stable in time (~ 2 seconds) and waveform, consisting in an impulsive positive pressure onset followed by a short decompressive phase. The single pulse lasts less than 1 seconds (~ 0.5 s) and has a ~3.5 Hz of peak frequency. The intensity varies between 1 and 10 Pa at ~500 m of distance from source. Average daily amplitude during the 2003-2007 period ranges from 1 to 6 Pa, with a mean of ~2.2 Pa typical of mild degassing activity. Besides their stability, during period of wide amplitude variation the intermittent regime shows an inverse relation

between the time delay and the average amplitude, indicating that the regime of active degassing is driven by the gas flux within the shallow magma column.

The rapid gas expansion at the magma free surface has been invoked to explain the source of infrasonic puffing. By using this physical source model the gas output produced by a single infrasonic puffing has been estimated by assuming i) a simple, monopole, point source (rapid gas expansion) elastically propagating on atmosphere at 340 m/s, and ii) the propagation effects negligible at a recording distance of ~ 500 m. Single gas burst produces 40-160 kg of gas mass, resulting in an daily average during mild strombolian activity of ~ 1600 tons/day. Considering mean gas composition of plume at Stromboli, this value corresponds to an SO₂ mass output of ~ 100 tons/day. The active degassing accounts at least for the $\sim 38\%$ of the total SO₂ output at Stromboli, indicating an efficient mechanism of gas loss through the shallow system of conduits in overpressurized condition.

During the analyzed period, the observed dynamics of source location indicates that active degassing is exclusive of only one single vent at once within the three main active vents (SW, C and NE). This behaviour seems to be consistent with experimental and numerical studies on the partitioning of particles and drops at pipe bifurcations, where train of bubbles flows within the major gas flux path. The presence of a permanent multiparametric network at Stromboli moreover, allows a long-term (2003-2007) analysis during variable volcanic activity, from mild to high, and the 2007 explosive to effusive transition phase. During this period puffing was located mainly in the Central vent. However, shifts in location were observed from C to NE vent, while only in few cases was moving to the South-West vent (SW). Active degassing at Stromboli, would thus not only reflects the higher gas flux regimes in the shallow conduit but it will indicate where the gas flux is more localized within the shallow volcanic system.

Based on the results of the infrasonic array analysis, a schematic model for active degassing at Stromboli has been proposed. A NE-SW striking dike with $\sim 60^\circ$ of dip toward NW has been considered based on geo-structural and geophysical constrains. The uppermost portion of such dike has been imaged as a system of vertical conduits connecting the magma to the surface. Accumulation of exsolved gas at depth has been suggested as the source of the excess pressure observed at surface as explosive activity. This is a plausible explanation for the high gas to mass fraction (~ 16 in mass) observed

during both active degassing and explosions. The low CO_2/SO_2 ratio (< 10) observed in the plume during mild degassing is consistent with a gas source at a pressure of less than 4 MPa (150 m). The intense vesiculation process and the formation of a gas pocket should be active at such depth within the shallow magmatic column, which is consistent with the seismic source. Laboratory experiments where gas bubbles accumulate at the top of a tank filled with viscous fluid and topped by small vertical conduit, reproduce a steady-state intermittent regime that finds great consistence with the regime of active degassing. This model has been used here to calculate the dike dimension that could explain the gas flux regime inferred from infrasonic analysis. This analysis indicates that the steady-state regime of active degassing can be explained by the collapse of a foam volume confined in a 10 m thick and 120-170 m length dike where accumulate 0.3-0.5 mm large gas bubbles. This dike length is consistent with the dimension of the crater rim (~ 220 m) and also explains the common variation of the explosive rate observed at the three main active vents.

The model proposed for the sustained degassing of the shallow magmatic column at Stromboli finds additional evidence in the dynamics observed during the 2007 eruption. The opening of a NE-SW fissure at Stromboli is interpreted here as a consequence of the increase of the magma input rate above the typical $0.3 \text{ m}^3/\text{s}$ rate. A significant increase of the magma input rate has been already observed 1 month before the onset of the 2007 eruption, as indicated by the increase (from 8 to 14 explosions/hours) of the explosive rate. This precursory phase was followed by an increment in intensity and a migration toward NE of the location of the active degassing. This is here interpreted as an increase in the gas flux rate inducing an increase in the degassing mechanism. However, when the magma input rate exceeded the threshold value of $0.3 \text{ m}^3/\text{s}$ the shallow conduits system was not able anymore to support the large volumetric increment and started to fracture. The migration toward NE indicates a modification of the gas streamlines within the shallow conduits, and can be the evidence of such instability. Hence, the NE migration indicates the location of where the large magma input rate is concentrated and correspond to the weak zone inside the shallow feeding system, where the lava effusion was taking place. Migration and dynamic of active degassing as well as explosive centres have been observed during days before the onset of the eruption.

This work aimed to demonstrate the capability and contribution of the infrasonic method to the study complex volcanic process. On open vents volcanoes, such Stromboli, small aperture infrasonic array allows not only to monitor the volcanic activity, but can help to identify and quantify the gas flux mechanism and its regime, providing valuable information on the way magma moves in the shallow portion of the feeding system.

6. References

- Aiuppa A., Federico C., Giudice G., Giuffrida G., Guida R., Guerrieri S., Liuzzo M., Moretti M., Papale P., 2008. The 2007 eruption of Stromboli volcano: insight from real-time measurements of the volcanic gas plume CO₂/SO₂ ratio. *J. Volcanol. & Geotherm. Res.*, doi: 10.1016/j.jvolgeores.2008.09.013.
- Allard P., Carbonnelle J., Metrich N., Loyer H., and Zettwoog P., 1994. Sulfur output and magma degassing budget of Stromboli volcano. *Nature*, 368, pp. 326-330.
- Allard P., 1997. Endogenous magma degassing and storage at Mount Etna. *Geophys. Res. Lett.*, 24(17), pp. 2219-2222.
- Allard P., Carbonelle J., Dajlevic D., Le Bronec J., Morel P., Robe M.C., Maurenas J.M., Faivre-Perrat R., Martin D., Saubrox J-C., Zettwoog P., 1991. Eruptive and diffusive emissions of CO₂ from Mount Etna. *Nature*, 351, pp. 387-391.
- Anderson A. T., 1974. Chlorine, sulfur and water in magmas and oceans. *Am. Bull. Geol. Soc.*, 85, pp. 1485–1492.
- Andres R. J., W. I. Rose, P. R. Kyle, S. deSilva, P. Francis, M. Gardeweg, and H. Moreno Roa, 1991. Excessive sulfur dioxide emissions from Chilean volcanoes. *J. Volcanol. Geotherm. Res.*, 46, pp. 323–329.
- Aster R., W. McIntosh, P. Kyle, R. Esser, B. Bartel, N. Dunbar, B. Johns, J. Johnson, R. Karstens, C. Kurnik, M. McGowan, S. McNamara, C. Meertens, B. Pauly, M. Richmond and M. Ruiz, 2004. Real-time data received from Mount Erebus volcano, Antarctica. *Eos Trans. AGU*, 85, pp. 97, pp. 100-101.
- Barberi F., M. Rosi, and A. Sodi, 1993. Volcanic hazard assessment at Stromboli based on review of historical data. *Acta Vulcanol.*, 3, pp. 173–187.
- Bonaccorso S., S. Calvari, G. Gafri, L. Lodato, and D. Patanè, 2003. Dynamics of the December 2002 flank failure and tsunamis at Stromboli volcano inferred by volcanological and geophysical observations. *Geophys. Res. Lett.*, 30(18) 1941, doi 10.1029:2003GL017702.
- Braun T., and M. Ripepe, 1993. Interaction of seismic and air waves as recorded at Stromboli Volcano. *Geophys. Res. Lett.*, 20, pp. 6568-6571.
- Bruno N., Caltabiano T., Romano R., 1999. SO₂ emissions at Mt. Etna with particular reference to the period 1993–1995. *Bull. Volcanol.*, 60, pp. 405-411.

- Buckingham M. J., and M. A. Garcès, 1996. Canonical model of volcano acoustics. *J. Geophys. Res.*, 101, pp. 8129-8151.
- Burton M., P. Allard, L. Brusca, and F. Mure`, 2001. High resolution spectroscopic analysis of volcanic gas composition during passive and explosive degassing at Stromboli volcano, Italy, paper presented at the Assembly, Eur. Geophys. Soc., Nice, France, 25 March.
- Burton M., Allard P., Murè F., La Spina A., 2007a. Magmatic gas composition reveal the source depth of slug-driven Strombolian explosive activity. *Science*, 317, pp. 227-230.
- Calvari S., L. Spampinato, L. Lodato, A.J.L. Harris, M.R. Patrick, J. Dehn, M.R. Burton, and D. Andronico, 2005. Chronology and complex volcanic processes during the 2002 – 2003 flank eruption at Stromboli volcano (Italy) reconstructed from direct observations and surveys with handheld thermal camera. *J. Geophys. Res.*, 110, B02201, doi:10.1029/2004JB003129.
- Cansi Y., 1995. An automatic seismic event processing for detection and location. The P.M.C.C. method. *Geophys. Res. Lett.*, 22(9), 1021-1024.
- Chouet B., 1985. Excitation of a buried magmatic pipe: a seismic source model of volcanic tremor. *J. Geophys. Res.*, 90, 1881-1893.
- Chouet B., Hamisevicz N. and Mcgetchin T. R., 1974. Photoballistics of volcanic jet activity at Stromboli, Italy. *J. Geophys. Res.*, 79, pp. 4961–4976.
- Cramer O., 1993. The variation of the specific heat ratio and the speed of sound in air with temperature, pressure, humidity and CO₂ concentration. *J. Acoust. Soc. Am.*, 93, 2510-2516.
- Delle Donne D., Lacanna G., Marchetti M., Ripepe M., Ulivieri G., 2006. Monitoring Explosive Volcanic Activity Using Thermal Images, Stromboli Volcano, Italy. AGU Fall Meeting 2006, poster.
- De Groot-Hedlin C., 2005. Modeling infrasound waveforms in a windy Environment. *Inframatrics*, 11, pp. 1-7.
- Devine, J.D., Sigurdsson, H. and Davis, A.N., 1984. Estimates of sulfur and chlorine yield to the atmosphere from volcanic eruptions and potential climatic effects. *J. Geophys. Res.* 89, pp. 6309–6325.
- Ditchfield, R., and W.L. Olbricht, 1996. Effects of particle concentration on the partitioning of suspensions at small divergent bifurcations. *J. Biomech. Eng.*, 118(3), 287-294.
- Druitt T.H., Mellors R.A., Pyle D.M. and Sparks R.S.J., 1989. Explosive volcanism on Santorini. Greece. *Geol. Mag.* 126 2, pp. 95–213.

- Evers L.G., and H.W. Haak, 2003. Tracing a meteoric trajectory with infrasound. *Geophys. Res. Lett.*, 30(24), 2246, doi:10.1029/2003GL017947.
- Finizola A., F. Sortino, J.F. Lenat, and M. Valenza, 2002. Fluid circulation at Stromboli volcano (Aeolian Islands, Italy) from self-potential and CO₂ surveys. *J. Volcanol. Geotherm. Res.*, 116, pp. 1–18.
- Firstov P.P. and N.M. Kravchenko, 1996. Estimation of the amount of explosive gas release in volcanic eruption using air waves. *Volcanol. Seismol.*, 17, pp. 547-560.
- Ford R.D., 1970. *Introduction to acoustic*. Elsevier, New York, 154 pp.
- Francis P., C. Oppenheimer, and D. Stevenson, 1993. Endogenous growth of persistently active volcanoes. *Nature*, 366, pp. 554–557.
- Garcès M., A. Harris, C. Hetzer, J. Johnson, S. Rowland, E. Marchetti, and P. Okubo, 2003a. Infrasonic tremor observed at Kilauea Volcano, Hawai'i. *Geophys. Res. Lett.*, 30(20), 2023, doi:10.1029/2003GL018038.
- Garcès M., C. Hetzer, M. Merrifield, M. Willis, and J. Aucan, 2003b. Observations of surf infrasound in Hawai'i. *Geophys. Res. Lett.*, 30(24), 2264, doi:10.1029/2003GL018614.
- Garcès M., R.A. Hansen, and K.G. Lindquist, 1998. Traveltimes from infrasonic waves propagating in a stratified atmosphere. *Geophys. J. Int.*, 135, 255-263.
- Gerlach T.M., and Graeber, E.J., 1985. Volatile budget of Kilauea Volcano. *Nature*, 313, pp. 273-277.
- Gerlach T.M., 1986. Exolution of H₂O, CO₂, and S during eruptive episodes at Kilauea volcano, Hawaii. *J. Geophys Res*, 91(B12), pp. 12177–12185.
- Gerlach T.M., K.A. McGee, A.J. Sutton, and T. Elias, 1998. Rates of volcanic CO₂ degassing from airborne determinations of SO₂ emission rate and plume CO₂/SO₂: Test study at Pu'u'Ō'o cone, Kilauea volcano, Hawaii. *Geophys. Res. Lett.*, 25(14), pp. 2675–2678.
- Gilberti G., Jaupart, C., Sartorius G., 1992. Steady state operation of Stromboli volcano, Italy: constraints on the feeding system. *Bull. Volcanol.* 54, pp. 535-541.
- Harris A., J. Johnson, K. Horton, H. Gabriel, H. Ramm, E. Pilger, L. Flynn, P. Mouginiis-Mark, D. Piere, S. Donegan, D. Rothery, M. Ripepe, and E. Marchetti, 2003. Ground-based infrared monitoring provides new tool for remote tracking of volcanic activity. *Eos Trans. AGU*, 84, pp. 409-418.
- Harris A.J.L., and M. Ripepe, 2006. Multi-parametric approaches to measuring and understanding explosive volcanic phenomena: a case study from Stromboli. *Invited Review Article*, submitted.

- Harris A. J. L., and D. S. Stevenson, 1997. Thermal observations of degassing open conduits and fumaroles at Stromboli and Vulcano using remotely sensed data. *J. Volcanol. Geotherm. Res.*, 76, 175–198.
- Hedlin M., M. Garcés, H. Bass, C. Hayward, E. Herrin, J. Olson, and C. Wilson, 2002. Listening to the secret sounds of Earth's atmosphere. *Eos Trans. AGU*, vol. 83, pp. 557, 564-565.
- Jaupart C. and S. Vergnolle, 1989. The generation and collapse of a foam layer at the roof of a basaltic magma chamber. *J. Fluid Mech.*, vol. 203, pp. 347-380.
- Jaupart C. and S. Vergnolle, 1988. Laboratory models of Hawaiian and Strombolian eruptions. *Nature*, 331, pp. 58-60.
- Johnson J. B., and J.M. Lees, 2000. Plugs and chugs – seismic and acoustic observations of degassing exposures at Karymnsky, Russia and Sangay, Ecuador. *J. Volcanol. & Geotherm. Res.*, 101, pp. 67-82.
- Johnson J. B., 2004. Vent mapping and source location variability at Stromboli mapped with small-aperture infrasound-array. *Bull. Volcanol.*, doi:10.1007/s00445-004-0356-8.
- Johnson J. B., R.C. Aster, M.C. Ruiz, S.D. Malone, P.J. McChesney, J.M. Lees, and P.R. Kyle, 2003. Interpretation and utility of infrasonic records from erupting volcanoes. *J. Volcanol. Geotherm. Res.*, 121, 15-63.
- Kazahaya K., H. Shinohara, and G. Saito, 1994. Excessive degassing of Izu-Oshima volcano: Magma convection in a conduit. *Bull. Volcanol.*, 56, pp. 207–216.
- Lay T. and Wallace T., 1995. *Modern global seismology*. Academic Press, San Diego, 521 pp.
- Lees J. M., E. I. Gordeev, and M. Ripepe, 2004. Explosions and periodic tremor at Karymnsky volcano, Kamchatka, Russia. *Geophys. J. Int.*, 158, 1151–1167.
- Lighthill M.J., 1978. *Waves in Fluids*. Cambridge University Press, New York, 504 pp..
- Manga M., 1996. Dynamics of drops in branched tubes. *J. Fluid. Mech.*, 189, 105-117.
- Marchetti E., M. Ichihara, M. Ripepe, 2004. Propagation of acoustic waves in a viscoelastic two-phase system: influence of gas bubble concentration. *J. Volcanol. & Geotherm. Res.*, 137, 93-108.
- Marchetti E., Ripepe M., Caffo S., Ulivieri G., 2008. Infrasonic imaging of the shallow feeding system at Etna volcano. *Geophys. Res. Lett.*, submitted.
- Marchetti E., Genco R., Ripepe M., 2008. Ground deformation and seismicity related to the propagation and drainage of the dyke feeding system during the 2007 effusive eruption at Stromboli volcano (Italy). *J. Volcanol. & Geotherm. Res.*, doi:10.1016/j.jvolgeores.2008.11.016.

- Marchetti E., Delle Donne D., Genco R., Garaebiti E., Ripepe M., 2008. Integrated geophysical analysis of explosive activity at Yasur volcano, Vanuatu. AGU Fall Meeting 2008, poster.
- Menyailov I.A., Nikitina L.P., Shapar V.N., Pilipenko V.P., 1986. Temperature increase and chemical change of fumarolic gases at Momotombo Volcano, Nicaragua, in 1982–1985: are these indicators of a possible eruption?. *J. Geophys Res*, 91, pp. 12199–12214.
- Metrich N., Bertagnini A., Landi P., Rosi M., 2001. Crystallization driven by decompression and water loss at Stromboli volcano (Aeolian Islands Italy). *Journal of Petrology* 42 (8), pp. 1471–1490.
- Neuberg J., 2000. Characteristics and causes of shallow seismicity in andesite volcanoes. In: Francis, P., Neuberg, J., Sparks, R.S.J. (Eds.). *The causes and consequences of eruptions of andesite volcanoes*. *Philos. Trans. R. Soc.* 358, 1533-1546.
- Olson J.V., C.R. Wilson, and R.A. Hansen, 2003. Infrasound associated with the 2002 Denali fault earthquake, Alaska. *Geophys. Res. Lett.*, 30(23), 2195, doi:10.1029/2003GL018568.
- Papale P., 2005. Determination of total H₂O and CO₂ budgets in evolving magmas from melt inclusion data. *J. Geophys. Res.*, 110, doi:10.1029/2004JB003033.
- Pino A., M. Ripepe, and G.B. Cimino, 2004. The Stromboli volcano landslides of December 2002: A seismological description. *Geophys. Res. Lett.*, 31, L02605, doi:10.1029/2003GL018385.
- Proussevitch A.A., Sahagian D.L., Anderson A.T., 1993. Dynamics of diffusive bubble growth in magmas: isothermal case. *J. Geophys. Res.*, 98, pp. 22,283-22,307.
- Richards A.F., 1963. Volcanic sounds: Investigation and analysis. *J. Geophys. Res.*, 68, pp. 919-928.
- Ripepe M., M. Rossi and G. Saccorotti, 1993. Image analysis of the dynamical behavior at Stromboli. *J. Volcanol. Geoth. Res.*, 54, 335-351.
- Ripepe M., A. Harris, and R. Carniel, 2002. Thermal, Seismic and Infrasonic Insights into Conduit Process at Stromboli volcano. *J. Volcanol. & Geotherm. Res.*, 118, 285-207.
- Ripepe M., Poggi P. and Marchetti M., 2004. Small aperture infrasonic array monitors activity of Stromboli volcano. *Inframatrics*, 7, pp. 1-15.
- Ripepe M., and E. Gordeev, 1999. Gas bubble dynamics model for shallow volcanic tremor at Stromboli. *J. Geophys. Res.*, 104(B5), pp. 10,639-10,654.
- Ripepe M., Harris A., Marchetti M., 2005. Coupled thermal oscillations in explosive activity at different craters of Stromboli volcano. *Geophys. Res. Lett.*, 32, L17302, doi: 10.1029/2005GL022711.

- Ripepe M. and E. Marchetti, 2002. Array tracking of infrasonic sources at Stromboli volcano, *Geophys. Res. Lett.*, 29(22), 2076, doi:10.1029/2002GL015452.
- Ripepe M., E. Marchetti, G. Ulivieri, A. Harris, J. Dehn, M. Burton, T. Caltabianco, and G. Salerno, 2005. Effusive to explosive transition during the 2003 eruption of Stromboli volcano. *Geology*, 33, 5, pp. 341-344.
- Ripepe M., E. Marchetti, P. Poggi, A. Harris, A. Fiaschi and G. Ulivieri, 2004. Seismic, acoustic and thermal network tracks in real time the 2003 eruption of Stromboli Volcano. *EOS Trans. AGU*, 85 (35), pp. 329-332.
- Ripepe M., Poggi P., Braun T., and Gordeev E., 1996. Infrasonic waves and volcanic tremor at Stromboli. *Geophys. Res. Lett.*, 23, pp. 181-184.
- Ripepe M., De Angelis S., Lacanna G., Poggi P., Williams C., Marchetti M., Delle Donne D., Ulivieri G., 2008. Infrasonic Tracking of Pyroclastic flows at Soufrière Hills volcano, Montserrat, WI. AGU Fall Meeting 2008, poster.
- Rosi M., A. Bertagnini and P. Landi, 2000. Onset of the persistent activity at Stromboli volcano (Italy). *Bull. Volcanol.*, 62, pp. 294–300.
- Rowe C.A., R.C. Aster, P.R. Kyle, R.R. Dibble, J.W. Schlue, 2000. Seismic and acoustic observations at Mount Erebus volcano, Ross Island, Antarctica, 1994-1998. *J. Volcanol. & Geotherm. Res.*, 101, pp. 105-128.
- Ruiz M.C., J.M. Lees, and J.B. Johnson, 2006. Source constraints of Tungurahua volcano explosion events. *Bull. Volcanol.*, doi:10.1007/s00445-005-0023-8.
- Salerno G., M. Burton T., Caltabianco E., Longo F. Mure, and D. Condarelli, 2004. Insights into the 2002–2003 eruption of Stromboli from daily measurements of SO₂ emission rates, *Geophys. Res. Abstr.*, 6, 04175.
- Stark J., and M. Manga, 2000. The motion of long bubbles in a network of tubes. *Transport in Porous Media*, 40, 201-218.
- Stevenson D.S., 1992. Heat transfer in active volcanoes: models of crater lake systems. PhD thesis, Open University, UK, pp. 1–235.
- Stevenson D.S., Blake S., 1998. Modelling the dynamics and thermodynamics of volcanic degassing. *Bull. Volcanol.*, 60, pp. 307–317.
- Stix J., 2007. Stability and instability of quiescently active volcanoes: the case of Masaya, Nicaragua. *Geology*, 35, pp. 535-538.
- Stoiber R. E., Malinconico, L. L., and Williams, S. N., 1983. Use of the correlation spectrometer at volcanoes. In *Forecasting Volcanic Events*. Edited by H. Tazieff and J. C. Sabroux (New York: Elsevier), pp. 425-444.

- Tibaldi A., 2001. Multiple sector collapses at Stromboli Volcano, Italy: How they work. *Bull. Volcanol.*, 63, pp. 112–125.
- Truax B., 1978. *The World Soundscape Project's Handbook for Acoustic Ecology*. A.R.C. Publications, Vancouver, 171 pp.
- Vergniolle S. and G. Brandeis, 1994. Origin of the sound generated by Strombolian explosions. *Geophys. Res. Lett.*, 21, 1959–1962.
- Vergniolle S. and G. Brandeis, 1996. Strombolian explosions, 1, A large bubble breaking at the surface of a lava column as a source of sound. *J. Geophys. Res.*, 101(B09), 20433–20448.
- Vergniolle S., G. Brandeis, and J.-C. Marechal, 1996. Strombolian explosions, 2, Eruption dynamics determined from acoustic measurements. *J. Geophys. Res.*, 101(B09), 20449–20466.
- Walker D. and O. Mullins Jr., 1981. Surface tension of natural silicates from 1200–1500. *Contrib. Mineral. Petrol.*, 76, pp. 455–462.
- Woods A.W., Koyaguchi T., 1993. Transitions between explosive and effusive eruptions of silicic magmas. *Nature*, 370, pp. 641–644.
- G. Zreda-Gostynska, P.R. Kyle and D. Finnegan, 1993. Chlorine, fluorine, and sulfur emissions from Mount Erebus, Antarctica and estimated contributions to the Antarctic atmosphere, *Geophys. Res. Lett.*, 20, pp. 1959–1962.
-